



HAL
open science

Robust Control of a Brain-Persisting Parasite through MHC I Presentation by Infected Neurons

Anna Salvioni, Marcy Belloy, Aurore Lebourg, Emilie Bassot, Vincent Cantaloube-Ferrieu, Virginie Vasseur, Sophie Blanié, Roland Liblau, Elsa Suberbielle, Ellen Robey, et al.

► **To cite this version:**

Anna Salvioni, Marcy Belloy, Aurore Lebourg, Emilie Bassot, Vincent Cantaloube-Ferrieu, et al.. Robust Control of a Brain-Persisting Parasite through MHC I Presentation by Infected Neurons. Cell Reports, 2019, 27 (11), pp.3254-3268.e8. 10.1016/j.celrep.2019.05.051 . hal-02374306

HAL Id: hal-02374306

<https://hal.science/hal-02374306>

Submitted on 25 Oct 2021

HAL is a multi-disciplinary open access archive for the deposit and dissemination of scientific research documents, whether they are published or not. The documents may come from teaching and research institutions in France or abroad, or from public or private research centers.

L'archive ouverte pluridisciplinaire **HAL**, est destinée au dépôt et à la diffusion de documents scientifiques de niveau recherche, publiés ou non, émanant des établissements d'enseignement et de recherche français ou étrangers, des laboratoires publics ou privés.



Distributed under a Creative Commons Attribution - NonCommercial 4.0 International License

Salvioni *et al.*

1 **Robust control of a brain-persisting parasite through MHC I presentation by infected neurons**

2

3 Anna Salvioni¹, Marcy Belloy¹, Aurore Lebourg¹, Emilie Bassot¹, Vincent Cantaloube-Ferrieu¹,
4 Virginie Vasseur¹, Sophie Blanié¹, Roland S. Liblau¹, Elsa Suberbielle¹, Ellen A. Robey², Nicolas
5 Blanchard^{1*}

6

7 ¹ Center for Pathophysiology Toulouse-Purpan (CPTP), INSERM, CNRS, University of Toulouse,
8 31024 Toulouse, France

9 ² Department of Molecular and Cell Biology, University of California, Berkeley, CA 94720, USA

10

11 * Address correspondence to Nicolas Blanchard, nicolas.blanchard@inserm.fr

12 CPTP INSERM U1043 - CHU Purpan - BP3028 – 31024 Toulouse Cedex 3 – France

13

14 Lead contact: Nicolas Blanchard, nicolas.blanchard@inserm.fr

15

16 **Summary**

17
18 Control of central nervous system (CNS) pathogens by CD8 T cells is key to avoid fatal
19 neuroinflammation. Yet the modalities of MHC I presentation in the brain are poorly
20 understood. Here we analyze the antigen presentation mechanisms underlying CD8 T cell-
21 mediated control of the *Toxoplasma gondii* parasite in the CNS. We show that MHC I
22 presentation of an efficiently processed model antigen (GRA6-OVA), even when not expressed
23 in the bradyzoite stage, reduces cyst burden and dampens encephalitis in C57BL/6 mice.
24 Antigen presentation assays with infected primary neurons reveal a correlation between lower
25 MHC I presentation of tachyzoite antigens by neurons and poor parasite control *in vivo*. Using
26 conditional MHC I-deficient mice, we find that neuronal MHC I presentation is required for
27 robust restriction of *T. gondii* in the CNS during chronic phase, showing the importance of MHC I
28 presentation by CNS neurons in the control of a prevalent brain pathogen.

29

30 **Introduction**

31 The brain is endowed with specialized innate and adaptive immune mechanisms that ensure
32 both the detection and mitigation of neurotropic infections (Klein and Hunter, 2017; Russo and
33 McGavern, 2015) but some pathogens can chronically reside within the central nervous system
34 (CNS). Accumulating evidence point to intricate links between neuroinflammation and the
35 development of neurodegenerative diseases (Colonna and Butovsky, 2017; Heneka et al., 2015).
36 By eliciting various degrees of inflammation, chronically persisting CNS pathogens are likely to
37 influence brain processes, including age-related cognitive dysfunctions (Cabral et al., 2017;
38 McManus and Heneka, 2017; Mohle et al., 2016). A better understanding of the mechanisms by
39 which immune components of the CNS, such as CD8 T cells, detect and control persisting
40 microorganisms is needed not only to improve containment of these pathogens but also to
41 potentially alleviate detrimental effects of chronic infections on brain functions.

42 The protozoan intracellular parasite *Toxoplasma gondii* is a widespread foodborne pathogen
43 (Guo et al., 2016), which commonly infects humans. Due to the lack of an effective drug
44 targeting its encysted bradyzoite stage, this parasite cannot be cleared from the brain. Hence,
45 with a worldwide seroprevalence of ~30% (Pappas et al., 2009) that can reach up to 50% in
46 certain countries (Wilking et al., 2016), *T. gondii* is thought to reside in the brains of more than 2
47 billion individuals. Following dissemination of the rapidly-dividing tachyzoites in the host, the
48 parasite converts into slower-growing bradyzoites, which chronically persist within cysts in
49 muscles and in the CNS (Ferguson and Hutchison, 1987). In the CNS, multiple resident cell types
50 may be in contact with tachyzoites but neurons are the only cells supporting the development
51 of cysts (Cabral et al., 2016; Melzer et al., 2010), which are mostly found within intact host cells
52 (Ferguson and Hutchison, 1987).

53 The clinical outcome of *T. gondii* infection critically depends on the host immune status and
54 more specifically on a fully functional T cell compartment. In immunocompetent humans, acute
55 infection remains mildly symptomatic but chronic presence of *T. gondii* in the brain (referred to
56 as latent toxoplasmosis) has been associated with neuropsychiatric disorders, such as
57 schizophrenia (Torrey and Yolken, 2003) and cognitive changes (Stock et al., 2017), although

58 conflicting data exist on this question (Perry *et al.*, 2016; Wyman *et al.*, 2017). In rodents, which
59 are natural hosts of *T. gondii*, the parasite has been reported to influence the course of
60 neurodegenerative disorders (Cabral *et al.*, 2017; Mohle *et al.*, 2016) and to cause major
61 behavioral modifications (Vyas, 2015). In case of T cell lymphopenia or sub-optimal function
62 (e.g. due to HIV/AIDS or immune suppressive treatment), individuals become at risk of
63 developing *T. gondii* encephalitis (TE), a fatal neuroinflammatory disease that is still common
64 among HIV-infected people (Ondounda *et al.*, 2016). TE is characterized by high cyst burden,
65 tachyzoite replication foci in the CNS, massive immune cell influx, activation of recruited and
66 local myeloid cells and cerebral tissue damage (Parlog *et al.*, 2014). TE is also associated with
67 activation and exhaustion of CD4 T cells, leading to functional attrition of CD8 T cells (Hwang *et al.*,
68 2016).

69 Mouse studies have highlighted a variety of innate immune mechanisms that can contribute to
70 parasite control in the brain. These include the production of pro-inflammatory mediators by
71 innate mononuclear cells (Biswas *et al.*, 2015; Sa *et al.*, 2015) and neutrophils (Biswas *et al.*,
72 2017), as well as anti-microbial pathways triggered by IFN γ /STAT1 in astrocytes (Hidano *et al.*,
73 2016). Yet, these processes are typically not sufficient to prevent TE pathogenesis. In contrast,
74 CD8 T cells and MHC I, in particular the H-2 L^d MHC I allele, are pivotal to drive robust and
75 durable brain parasite control and to dampen encephalitis, a status known as TE resistance
76 (Blanchard *et al.*, 2008; Brown *et al.*, 1995). Consequently, C57BL/6 mice, which are devoid of
77 H-2 L^d, are a good model to study the pathogenesis of *T. gondii* encephalitis while mice
78 expressing H-2 L^d (e.g. BALB/c or congenic B6.H-2^d mice) are TE-resistant (Blanchard *et al.*,
79 2015). In mice bearing the H-2^d MHC haplotype, protection from TE relies on the induction of
80 CD8 T cells specific for an immunodominant L^d-restricted peptide that is efficiently processed
81 from the *T. gondii*-secreted GRA6 protein in infected macrophages and dendritic cells (DC)
82 (Blanchard *et al.*, 2008; Feliu *et al.*, 2013). This protective response is maintained without a
83 contraction phase, by continuous production of effector CD8 T cells *via* a proliferative, antigen-
84 dependent population, displaying a memory-effector hybrid phenotype (Chu *et al.*, 2016).
85 While induction of GRA6-specific peripheral CD8 T cell responses in the periphery is a clear

86 prerequisite to enable robust parasite control in the brain (Feliu et al., 2013), the determinants
87 underlying CD8-mediated surveillance of *T. gondii* in the CNS in the context of TE resistance
88 remain ill-defined.

89 To address this question without modifying the endogenous GRA6 protein, which plays a role in
90 cystogenesis (Fox et al., 2011), we created transgenic parasites ectopically expressing a model
91 antigen composed of the H-2 K^b-restricted OVA-derived SIINFEKL epitope in fusion with the C-
92 terminus of GRA6, a known immunogenic position (Feliu et al., 2013). Compared to parasites
93 expressing the same SIINFEKL epitope within a different source antigen (vacOVA), C57BL/6 mice
94 infected with the GRA6-OVA-expressing parasites displayed limited brain inflammation. Using a
95 promoter restricting expression of the GRA6-OVA antigen to tachyzoites, we showed that CD8 T
96 cell recognition of this antigen at the tachyzoite stage is enough to ensure parasite restriction in
97 the brain. Measurements of antigen presentation by primary neuronal cultures infected with
98 parasites leading to TE (vacOVA) or to a reduced CNS inflammation (GRA6-OVA) suggested the
99 implication of neuronal MHC I presentation in the control of brain parasite load. To formally
100 address this possibility, we developed a mouse model enabling selective ablation of the H-2 L^d
101 allele (naturally conferring resistance to TE) in neurons. Our results revealed that although
102 neuronal MHC I presentation is dispensable for CNS accumulation of *T. gondii*-specific CD8 T
103 cells, it is critical for durable parasite control.

104 **Results**

105 **A CD8 T cell-dependent TE-resistant model in C57BL/6 mice based on GRA6-OVA expression**

106 To study how CD8 T cell-mediated detection and restriction of *T. gondii* in the CNS are achieved,
107 we sought to create a C57BL/6-based model in which parasites expressing a tractable CD8 T cell
108 model antigen would be efficiently or poorly controlled at chronic phase, leading to limited vs.
109 active brain inflammation and thereby mimicking *T. gondii* latency vs. encephalitis. Since CD8 T
110 cell responses specific for the GRA6-derived HPGSVNEFDF (HF10) epitope are pivotal for
111 resistance to *T. gondii* encephalitis in H-2 L^{d+} mice (Blanchard *et al.*, 2008; Feliu *et al.*, 2013) and
112 since GRA6 C-terminus is a preferential location for antigenicity (Buillon *et al.*, 2017; Feliu *et al.*,
113 *et al.*, 2013), we reasoned that the addition of the H-2 K^b-restricted chicken ovalbumin (OVA)-
114 derived SIINFEKL model epitope to the C-terminus of GRA6 may protect C57BL/6 mice from the
115 CNS inflammation that is typically observed after infection by type II parasites. To test this
116 hypothesis, we generated type II parasites (Tomato⁺ Pru) expressing the GRA6-OVA model
117 antigen. In order to preserve the final antigen processing steps, the OVA-derived SIINFEKL
118 peptide was flanked by 5 amino acids that are naturally present in OVA (**Fig. 1a**). In parallel, we
119 took advantage of a previously described (Schaeffer *et al.*, 2009) Tomato⁺ Pru strain that
120 expresses the SIINFEKL epitope embedded in a different dense granule-secreted antigen: the
121 vacuolar SAG1ΔGPI-OVA protein (abbreviated here as vacOVA) (**Fig. 1a**). The resulting parasites
122 are designated as *Tg.pGRA6/GRA6-OVA* and *Tg.pTUB/vacOVA*, respectively. In line with the
123 known dual-stage activity of the tubulin and GRA6 promoters respectively controlling the
124 expression of vacOVA and GRA6-OVA, these two antigenic constructs were detected both in
125 tachyzoites and bradyzoites (Schaeffer *et al.*, 2009) (**Fig. 1a**). To ensure that the comparison of
126 these two transgenic parasites was valid, we evaluated the *in vivo* dissemination, access to the
127 brain and CD8 T cell responses elicited in the course of acute toxoplasmosis. Ten days post-
128 infection, comparable OVA-specific CD8 T cell responses were induced in the spleen by both
129 strains, which disseminated in the spleen and, even more efficiently than the parental strain, in
130 the brain (**Sup. Fig. 1a, b, c, d**). Yet 3 weeks post-infection, i.e. at the beginning of chronic stage,
131 the *Tg.pGRA6/GRA6-OVA* parasites were more robustly restricted in the CNS than the

132 *Tg.pTUB/vacOVA* parasites. Such a difference was observed in H-2^b (K^b-positive) C57BL/6, which
133 develop prominent SIINFEKL-specific CD8 T cell responses in the CNS (**Fig. 4d, e**), but not in H-2^k
134 (K^b-negative) CBA mice (**Fig. 1b, c, d and Fig S1e, f, g**). As CBA mice are unable to present the
135 SIINFEKL peptide, these data show (i) that the *in vivo* fitness of the *Tg.pGRA6/GRA6-OVA* is not
136 altered and (ii) that the beneficial impact of GRA6-OVA on CNS parasite control in C57BL/6 mice
137 is likely linked to H-2K^b-restricted CD8 T cell responses.

138 Next we assessed whether the lower load of *Tg.pGRA6/GRA6-OVA* in the CNS indeed correlated
139 with reduced brain inflammation. Besides a high cyst burden, the encephalitis caused by *T.*
140 *gondii* is typically characterized by foci of tachyzoite replication, activation of brain-resident
141 microglia and macrophages, infiltrates of activated lymphocytes and myeloid cells comprising
142 inflammatory monocytes and DC (Biswas *et al.*, 2015; Blanchard *et al.*, 2015; Hwang *et al.*, 2016;
143 John *et al.*, 2011; O'Brien *et al.*, 2019; O'Brien *et al.*, 2017; Zhang *et al.*, 2014). As a reflection of
144 the myeloid cell infiltrate, the relative abundance of brain-infiltrating CD11b⁺ CD45^{hi} over brain-
145 resident microglia (typically characterized as CD11b⁺ CD45^{int} at steady-state), was reduced in
146 mice infected with parasites expressing GRA6-OVA (**Fig. 1e, f**). Although the surface levels of
147 MHC II and CD86 on CD11b⁺ CD45^{int} microglia did not dramatically differ between the infected
148 groups at this time point (**Fig S1h, i, j, k**), Iba1⁺ cells were found accumulated in foci in the cortex
149 of mice infected with the parental or *Tg.pTUB/vacOVA* parasites (**Fig. 1g**). There was no
150 substantial difference in the level of CD86 expression on CD11b⁺ Ly6C^{hi} inflammatory monocytes
151 across the infected groups (**Fig S1l**) but the infiltration of inflammatory Ly6C^{hi} monocytes was
152 decreased in the brains *Tg.pGRA6/GRA6-OVA*-infected mice (**Fig. 1h**), which also displayed the
153 lowest proportion of monocyte-derived MHCII⁺ DC (**Fig. 1i**). At last, less activated IFN γ -
154 producing CD4 T cells were found in brains from *Tg.pGRA6/GRA6-OVA*-infected mice (**Fig. 1j**).
155 Together, these results indicate that, in comparison to the parental strain or to *vacOVA*-
156 expressing parasites, infection with GRA6-OVA-expressing type II *T. gondii* elicits efficient
157 parasite control in the CNS and reduced CNS inflammation. They establish a useful model to
158 study TE resistance in C57BL/6 mice.

159

160 **Comparable OVA-specific CD8 T cell responses elicited by GRA6-OVA when expressed by both**
161 **parasite stages or when restricted to tachyzoites**

162 Depending on the time post-infection (early dissemination vs. chronic stage) and the
163 immunological context examined (effective vs. poor parasite control), the CNS tissue can harbor
164 varying numbers of *T. gondii* tachyzoites and bradyzoites (Bhadra et al., 2013). In order to
165 examine which parasite stage(s) is/are efficiently held in check by CD8 T cells in the CNS in the
166 context of latent toxoplasmosis, we generated parasites where GRA6-OVA expression was
167 restricted to tachyzoites. To this aim, we drove expression of the GRA6-OVA antigen with the
168 SAG1 promoter, which is active only at the tachyzoite stage, thereby generating the
169 *Tg.pSAG1/GRA6-OVA* strain (**Fig. 2a**). Using two complementary assays, we confirmed that
170 GRA6-OVA was indeed shut-down in *Tg.pSAG1/GRA6-OVA* bradyzoites. First, tachyzoite-
171 infected fibroblasts were treated with apicidin, a histone deacetylase inhibitor which
172 upregulates several genes involved in bradyzoite conversion (Bougdour et al., 2009; Boyle et al.,
173 2006). We observed by Western blot that GRA6-OVA expression was lost in apicidin-treated
174 *Tg.pSAG1/GRA6-OVA* bradyzoites (**Fig. S2a, b**). Because only part of the bradyzoite
175 differentiation program is mimicked by apicidin treatment (Bougdour et al., 2009), we also
176 evaluated expression of the respective antigenic constructs in *ex vivo* isolated *bona fide* cysts.
177 GRA6-OVA could be visualized in *Tg.pGRA6/GRA6-OVA* cysts and, confirming the *in vitro* data, it
178 was not detectable in *Tg.pSAG1/GRA6-OVA* cysts (**Fig. 2b**).

179 Having validated the stage expression profile of these two antigenic constructs, we analyzed
180 MHC I presentation, CD8 T cell responses and dissemination to the brain during acute phase.
181 Using LacZ-inducible reporter CD8 T cell hybridomas that specifically respond to the K^b-SIINFEKL
182 MHC-peptide complexes (B3Z), we observed an equivalent presentation of the SIINFEKL peptide
183 by DC infected with tachyzoites, regardless of the promoter used (**Fig. 2c**), which was consistent
184 with a similar induction of OVA-specific CD8 T cell responses in the spleen 10 days post infection
185 (**Fig. S2c, d**). In addition, in this context, initial parasite invasion of the brain was not
186 substantially altered by the presence of GRA6-OVA compared to the parental strain (**Fig. S2e**).

187 We then proceeded to analyze CD8 T cell responses, parasite burden and CNS inflammation at
188 chronic phase. We chose to perform the analyses at late chronic phase, i.e. 2 months post-
189 infection, to limit the potential effects of pSAG1/GRA6-OVA residual expression that would be
190 expected in the early days of chronic phase, when bradyzoites have converted only recently.
191 Whether or not GRA6-OVA was expressed in bradyzoites, both strains elicited comparable CD8 T
192 cell responses to the SIINFEKL peptide in the spleen and brain (**Fig. 2d, e, f, h, i**). CD8 T cells
193 specific for another K^b-restricted peptide, the Tgd057-derived SVLAFRRL epitope, were found in
194 similar proportions in the 3 groups in the spleen and were slightly more abundant in the brains
195 of mice infected with the parental *Tg.GFP* (**Fig. 2e, g, h, j**). In conclusion, CD8 T cell responses
196 developing against a *T. gondii* tachyzoite-restricted antigen are maintained throughout chronic
197 infection, even in the absence of antigen expression by bradyzoites.

198 **Tachyzoite-restricted GRA6-OVA expression is sufficient to provide robust CNS parasite**
199 **control and to dampen TE**

200 We next assessed the impact of tachyzoite-restricted GRA6-OVA expression on brain parasite
201 control and TE pathogenesis (**Fig. 3a**). Compared to the parental strain, we observed a major
202 reduction in brain cysts (**Fig. 3b**) and parasite DNA (**Fig. 3c**) in C57BL/6 mice infected with *T.*
203 *gondii* expressing GRA6-OVA independently from the promoter. Consistent with brain parasite
204 control being primarily mediated by K^b-OVA-specific CD8 responses (see Fig. 1d), parasite
205 burdens were similar in chronically infected TE-susceptible H-2^k CBA mice (**Fig. 3d**). In order to
206 assess TE pathogenesis, we evaluated the CNS immune infiltration and activation of myeloid and
207 CD4 T cells. Regardless of the promoter, mice infected with GRA6-OVA-expressing strains
208 displayed a lower ratio of CD11b⁺ CD45^{hi} inflammatory myeloid cells over CD11b⁺ CD45^{int}
209 microglia (**Fig. 3e, f**) and microglial populations were less activated, as evidenced by reduced
210 CD86 and MHC II surface expression (**Fig. 3g, h**). We observed a less pronounced accumulation
211 of CD11b⁺ Ly6C^{hi} inflammatory monocytes (**Fig. 3i**), which displayed a lower, though not
212 significant, level of CD86 expression (**Fig. 3j**) and among which there were fewer differentiated
213 MHC II⁺ DC (**Fig. 3k**). At last, these brains contained less IFN γ -producing CD4 T cells (**Fig. 3l**).

214 These results show that C57BL/6 mice infected with *Tg.pGRA6/GRA6-OVA* and *Tg.pSAG1/GRA6-*
215 *OVA* have reduced brain inflammation, in contrast to mice infected with parental *Tg.GFP*.

216 Altogether, this set of data indicates that CD8 T cell recognition of an efficiently processed
217 tachyzoite-derived antigen is sufficient to provide effective parasite control in the CNS, thereby
218 limiting the development of TE.

219 **Limited TE development conferred by GRA6-OVA expression correlates with efficient neuronal** 220 **MHC I presentation**

221 We next sought to gain further insights into the modalities of MHC I presentation within the
222 CNS, in particular regarding the nature of the antigen-presenting cells that determine the
223 pathogenesis of TE. To this aim, we took advantage of the *Tg.pTUB/vacOVA* and
224 *Tg.pGRA6/GRA6-OVA* parasite strains described in Figure 1, which express the same CD8 T cell
225 epitope embedded in differentially protective source antigens, leading to varying levels of
226 parasite control and CNS inflammation. We first interrogated whether the poor containment of
227 *Tg.pTUB/vacOVA* parasites compared to *Tg.pGRA6/GRA6-OVA* could be due to improper
228 recruitment and activation of OVA-specific CD8 T cells in the cerebral tissue. In contrast to the
229 experiments in which the GRA6-OVA antigen was restricted to tachyzoites (see Fig. 2 and 3),
230 there was no concern about residual antigen expression in the early chronic phase.

231 Furthermore, the differences in brain parasite burden and inflammation of Figure 1 were
232 observed at 3 weeks post-infection. Therefore, we assessed the abundance, specificity and
233 effector functions of splenic and brain-infiltrating CD8 T cells 3 weeks post-infection (**Fig. 4a**). In
234 the spleen, substantial SIINFEKL-specific CD8 T cells were elicited by both GRA6-OVA- and
235 vacOVA-expressing parasites, with a slightly higher magnitude in the context of
236 *Tg.pGRA6/GRA6-OVA* infection (**Fig. 4b, c**). In the brain, the numbers of K^b-SIINFEKL dextramer⁺
237 CD8 T cells and of IFN γ -producing CD8 T cells after SIINFEKL peptide restimulation were similar
238 between *Tg.pTUB/vacOVA* and *Tg.pGRA6/GRA6-OVA*-infected mice (**Fig. 4d, e**). Analysis of the
239 effector potential of OVA-specific CD8 T cells following *in vitro* peptide restimulation showed
240 that vacOVA-expressing parasites in fact led to larger quantities of triple-producing IFN γ ⁺ TNF⁺
241 granzyme B⁺ CD8 T cells (**Fig. 4f**). This may be related to the higher parasite burden observed in
10

242 this setting. A more abundant antigenic material could, *via* MHC I presentation by local APC,
243 accelerate CD8 T cell differentiation into effector cells. In conclusion however, poor control of
244 vacOVA-expressing parasites is not due to defective infiltration or impaired effector
245 differentiation of *T. gondii*-specific CD8 T cells in the infected CNS. On this ground, we
246 hypothesized that what may be subpar in the vacOVA context is the recognition of infected
247 target cells by CD8 T cells.

248 Neurons being the most predominant host cells for *T. gondii* in the CNS (Cabral *et al.*, 2016;
249 Ferguson and Hutchison, 1987; Melzer *et al.*, 2010), we speculated that inefficient neuronal
250 MHC I presentation of vacOVA compared to GRA6-OVA may underlie impaired parasite control.
251 To test this possibility, we set out to probe antigen presentation by primary neurons infected
252 with *Tg.pTUB/vacOVA* and *Tg.pGRA6/GRA6-OVA* tachyzoites using the SIINFEKL-specific LacZ-
253 inducible B3Z reporter CD8 T cell hybridomas (**Fig. 5a**). First, we optimized neuronal culture
254 conditions to ensure that the proportion of glial cells was minimal because these are potent
255 antigen-presenting cells that may blur the interpretation of the assay (**Fig. S3a, b**). We also
256 verified that 24 h post-infection, > 95% of the *T. gondii* tachyzoite-containing vacuoles were
257 harbored in neurons (**Fig. S3c**) and that there were no differences in neuronal infection rates
258 between the two parasite strains (**Fig. 5b, c**). Antigen presentation measurements revealed that
259 the GRA6-OVA antigen was processed and presented by H-2K^b to the reporter CD8 T cells more
260 efficiently than the vacOVA antigen (**Fig. 5d**).

261 These data support the notion that failure to control vacOVA-expressing parasites in the CNS
262 may be related to sub-optimal MHC I presentation of *T. gondii* tachyzoite antigens by infected
263 neurons.

264 **MHC I L^d selective ablation in neurons hampers control of parasite load in the CNS**

265 To formally address the *in vivo* requirement for neuronal MHC I antigen presentation in the
266 control of CNS parasites, we designed a Cre-loxP-based conditional deletion approach. Because
267 MHC I molecules play important functions during brain development and plasticity (Corriveau *et al.*
268 *al.*, 1998; Elmer and McAllister, 2012; Huh *et al.*, 2000), we reasoned that it would be

269 appropriate to leave the endogenous C57BL/6 MHC I locus intact while introducing a floxed
270 version of H-2 L^d, the allele that was originally associated with TE resistance (Blanchard *et al.*,
271 2008; Brown *et al.*, 1995). We thus generated transgenic B6.L^dLox mice expressing a floxed L^d
272 gene, in which exons 1 to 3 are flanked by LoxP sites (**Fig. 6a**). As expected, T cells, B cells and
273 DC in the spleen of B6.L^dLox mice displayed K^b levels that were analogous to C57BL/6 mice (**Fig.**
274 **6b**). Surface expression of L^d in B6.L^dLox mice was slightly reduced compared to B6.H-2^d
275 congenic mice, which naturally express H-2 L^d (**Fig. 6c**) but despite this, B6.L^dLox and B6.H-2^d
276 mice mounted robust CD8 T cell responses to the L^d-restricted *T. gondii* GRA6-derived HF10
277 peptide in the spleen and brain (**Fig. 6d, e, f**). Accordingly, compared to C57BL/6 mice, B6.L^dLox
278 mice were potent in their ability to control brain *T. gondii* during chronic infection (**Fig. 6g**).

279 In order to selectively eliminate L^d from neurons, we bred B6.L^dLox with B6.CamKII α -iCre mice,
280 which express the Cre recombinase in all excitatory glutamatergic neurons of the CNS
281 (forebrain, hippocampus, olfactory lobe and scattered cells in hypothalamus) (Casanova *et al.*,
282 2001; Wang *et al.*, 2013). In Cre⁺ mice, CamKII α ⁺ neurons should express only K^b and D^b
283 whereas all other cells should express K^b, D^b and L^d (**Fig. 6h**). The level of L^d on the surface of
284 leukocytes isolated from infected brains was indeed comparable regardless of Cre expression
285 (**Fig. S4a**). In addition, as shown in primary co-cultures of neuronal and glial cells from CamKII α -
286 Cre⁺ vs. CamKII α -Cre⁻ mice, L^d expression was significantly reduced in Cre⁺ neurons while it was
287 not changed in Cre⁺ glial cells (**Fig. S4b, c**). To monitor parasite-specific CD8 T cell responses, we
288 infected mice with a *T. gondii* strain that naturally carries the endogenous GRA6 and Tgd057
289 proteins but is devoid of the OVA antigen. Effector CD8 T cell responses specific for the GRA6-
290 derived L^d-restricted HPGSVNEFDF peptide and the Tgd057-derived K^b-restricted SVLAFRRL
291 peptide were elicited similarly in the periphery of Cre⁺ and Cre⁻ mice (**Fig. S5a, b, c**). Parasite
292 dissemination in the spleen, peritoneum and brain throughout acute infection was also
293 comparable in the presence or absence of L^d on neurons (**Fig. S5d, e, f**). To evaluate the impact
294 of L^d neuronal deletion during chronic infection, we infected mice *per os* with the 76K
295 unmanipulated strain, akin to what occurs during natural infection. On week 3 post-infection,
296 there was a >10-fold increase in brain parasite burden in mice devoid of L^d in neurons, reflected

297 both by elevated cyst numbers (**Fig. 6i, j**) and parasite DNA (**Fig. 6k**). Brain parasite control in
298 Cre⁺ mice was as poor as that observed in chronically infected TE-susceptible C57BL/6 mice (**Fig.**
299 **6j, k**), indicating that the selective absence of L^d on neurons critically impairs the ability of local
300 CD8 T cells to restrict CNS parasites. To check if L^d deficiency in neurons impeded the
301 development of cerebral CD8 T cell responses, we quantified the numbers of total CD8 T cells
302 and GRA6-specific CD8 T cells in chronically infected brains. Absence of L^d in neurons did not
303 abrogate the infiltration of total CD8 T cells (**Fig. 6l**), nor did it preclude the accumulation of
304 IFN γ -producing GRA6-specific CD8 T cells (**Fig. 6m**). Evaluation of the ratio of inflammatory
305 myeloid cells over microglia, of the activation status of microglia and of the IFN γ -producing CD4
306 T cells in the CNS did not reveal substantial differences between Cre⁻ and Cre⁺ animals (**Fig. S6**),
307 suggesting that at 3 weeks post-infection, neuronal presentation of *T. gondii* antigens by L^d
308 plays a limited role in regulating CNS inflammation. Altogether, our findings establish that
309 efficient MHC I presentation of immunodominant *T. gondii* antigen by tachyzoite-infected
310 neurons is dispensable for the accumulation of CD8 T cells in the CNS but is a prerequisite for
311 sustained parasite control by CD8 T cells in this organ.
312

313 **Discussion**

314 Combining transgenic *T. gondii* parasites, antigen presentation assays with primary neurons and
315 a mouse model of conditional MHC I deletion, our data support a model whereby the efficacy of
316 CD8 T cell-mediated surveillance of tachyzoite-infected neurons determines the severity of CNS
317 inflammation. Notably, C57BL/6 mice infected with GRA6-OVA-expressing parasites durably
318 control the parasite in the CNS and show limited encephalitis throughout late chronic infection.
319 Our work sheds light on the stage specificity of CD8 T cell-mediated surveillance of *T. gondii* in
320 the CNS. In the context of TE development, two-photon laser scanning microscopy imaging of
321 infected brains previously revealed that CD8 T cells contact granuloma-like structures containing
322 tachyzoites and that they interact in a cognate manner with individual CD11b⁺ or CD11c⁺
323 antigen-presenting cells (APC) that are not necessarily infected (John et al., 2011; Schaeffer et
324 al., 2009). It was also found that CD8 T cells largely ignore neurons harboring cysts (Schaeffer et
325 al., 2009), in line with the notion that, as ‘dormant’ persisting structures, cysts must be
326 impervious to host immunity. However bradyzoites within tissue cysts are dynamic and
327 replicative entities (Watts et al., 2015) and intra-neuronal cysts contain up to thousands of
328 bradyzoites that continue to express and secrete a number of proteins, some of which are major
329 CD8 T cell targets (e.g. ROP7 (Frickel et al., 2008) and GRA6). Therefore, in the context of latent
330 toxoplasmosis, a different scenario may prevail whereby CD8 T cells could directly recognize and
331 eliminate cysts. In accordance, it was reported in a TE reactivation model in which
332 immunodeficient BALB/c mice are treated with sulfadiazine, that following adoptive transfer,
333 total splenic CD8 T cells isolated from chronically infected mice could reduce cyst count through
334 a perforin-dependent, IFN γ -independent, *modus operandi* (Suzuki et al., 2010). Here, in the
335 course of primary infection of an immunocompetent host, we report that *T. gondii*-infected
336 neurons are able to process tachyzoite antigens and to display antigenic fragments *via* MHC I for
337 CD8 T cell recognition. This is then sufficient to restrict brain cyst load up to 2 months post-
338 infection, stressing the notion that CD8 T cell recognition of tachyzoite-derived antigens is a
339 prominent driver to limit the development of TE. In this model, we hypothesize that antigenic
340 peptides are displayed by neuronal MHC I as soon as a neuron gets infected by a tachyzoite and

341 that this is enough to trigger cytotoxic T lymphocyte (CTL)-mediated containment of the
342 parasite invader. An interesting implication is that in the context of TE resistance, the parasites
343 are controlled 'from the beginning' (as tachyzoites) and that bradyzoite conversion only
344 minimally occurs. It will now be essential to determine by which mechanisms bradyzoites
345 actively escape CD8 T cell surveillance, including in the context of the robust CD8 T cell
346 responses leading to reduced encephalitis. Current drugs are ineffective on cysts, hence being
347 able to restore presentation of bradyzoite antigens in order to boost cyst clearance by CD8 T
348 cells could ultimately open new therapeutic avenues for at-risk individuals.

349 Another asset of our work is the creation of a mouse model to genetically test the importance
350 of neuronal MHC I presentation in the control of *T. gondii* within the CNS. *In vitro* validation of
351 the B6.L^dLox model using primary neuronal cultures showed a selective reduction of L^d in
352 neurons compared to glial cells, but not a complete loss. The residual expression of L^d observed
353 in Cre⁺ neurons in this assay may be linked to the late and/or heterogenous expression of the
354 CamKII α promoter in *in vitro* cultures as well as to the half-life of the L^d protein following Cre-
355 mediated excision. Since our attempts to detect L^d directly on brain sections have not been
356 successful, one cannot exclude that a fraction of CamK-Cre⁺ neurons still retain L^d expression *in*
357 *vivo* following infection. Regardless, we found major consequences on parasite burden,
358 indicating that MHC I presentation by CamK α ⁺ excitatory glutamatergic neurons plays an
359 important role for the control of *T. gondii* in the CNS. Although initially controversial, it is now
360 indisputable that MHC I molecules are expressed by neurons, at the surface of both axons and
361 dendrites (Elmer and McAllister, 2012). Neuronal MHC I plays essential functions during brain
362 development by restricting the activity-dependent plasticity of connections (Huh et al., 2000)
363 and negatively regulating synaptic density (Glynn et al., 2011). In addition, several lines of
364 evidence support the notion that neuronal MHC I can present antigenic peptides and activate
365 CD8 T cells. Expression of a neo-antigen by neuronal subtypes, like the orexinergic neurons
366 (Bernard-Valnet et al., 2016) or Purkinje cells (Yshii et al., 2016), was associated with CTL
367 granule polarization and destruction of the neuron subset expressing the antigen. In viral
368 infections such as with Lymphocytic Choriomeningitis Virus (LCMV) (Kreutzfeldt et al., 2013; Rall

369 et al., 1995), Theiler's murine encephalomyelitis virus (McDole et al., 2010) and Borna disease
370 virus (Chevalier et al., 2011), CTL have been shown to interact with infected neurons in a MHC I-
371 and antigen-specific manner. Our work now demonstrates the essentiality of MHC I
372 presentation for effective CD8 T cell control of a widespread, non-viral, neurotropic pathogen.
373 What may be the outcome of neuronal MHC I presentation on neuron function? In certain
374 contexts, contacts of neurons with CTL lead to neuron killing (Bernard-Valnet et al., 2016;
375 Cebrian et al., 2014) but in other situations, they induce more subtle morphological changes,
376 such as an increase in membrane permeability (Chevalier et al., 2011), synaptic stripping (Di
377 Liberto et al., 2018) or a loss of axon integrity (Sauer et al., 2013), without triggering immediate
378 apoptosis. An alteration of electrical properties has also been reported (Meuth et al., 2009).
379 Future investigations should be undertaken to address whether cognate contacts between CTL
380 and *T. gondii*-infected neurons could result in alterations of the electrical activity of individual
381 neurons or integrated neuronal networks (Casanova et al., 2018). These experiments may
382 ultimately shed light on some mechanisms behind the behavioral alterations induced by *T.*
383 *gondii*.

384 Importantly, our study does not rule out important contributions from other CNS-resident cells
385 in regulating the course of toxoplasmosis *via* MHC I presentation of pathogen fragments. The
386 main impact of L^d deletion in neurons is to hamper parasite control but the consequences on
387 brain inflammation appear more modest. It does not seem so surprising since regardless of the
388 Cre status, L^d presentation is expected to remain intact in all other brain-resident and -
389 infiltrating populations, which are likely to be critical for T cell/myeloid cell infiltration. Chief
390 among these are microglia, which are potent antigen-presenting cells involved in regulating
391 effector and memory CD8 T cells that have reached the CNS (Colonna and Butovsky, 2017). In
392 chronically LCMV-infected mice, microglia act as a viral reservoir and they can be prompted to
393 present viral antigens that promote viral purge by CD8 T cells (Herz et al., 2015). In *T. gondii*-
394 infected CNS, microglia are activated in the vicinity of *T. gondii* replication foci during TE (Zhang
395 et al., 2014). Since L^d elimination from neurons only modestly impacted CD8 T cell
396 accumulation, it is tempting to speculate that L^d deletion from microglia would instead

Salvioni *et al.*

397 profoundly disrupt CD8 T cell infiltration and/or memory CD8 T cell formation in the brain.
398 Astrocytes is another cell type, which antigen-presenting function would deserve further
399 scrutiny (Wilson and Hunter, 2004). T cells may encounter astrocytes either in the parenchyma
400 or when crossing the blood-brain barrier endothelium that is surrounded by astrocytic endfeet.
401 Studies in viral infections uncovered a possible interplay between astrocytes and CD8 T cells (Xie
402 and Yang, 2015). Thanks to the above-described mouse model and to a recently published
403 floxed K^b system (Malo *et al.*, 2018), it will now be possible to explore the role(s) of MHC I
404 presentation by CNS-resident cells in homeostasis and disease. In the case of chronic *T. gondii*
405 infection, these models may be useful to better understand how brain function is impacted by
406 this widespread parasite.

407

408

409 **Acknowledgments**

410 F. L'Faqih-Olive, V. Duplan-Eche, A.-L. Iscache, L. de la Fuente for technical assistance at the
411 CPTP-Inserm U1043 flow cytometry facility ; S. Allart, A. Canivet-Laffitte, D. Daviaud for
412 technical assistance at the CPTP-Inserm U1043 imaging facility ; G. Tavernier and Y. Barreira at
413 INSERM UMS006-CREFRE for the generation of the B6.L^dLox mice, R. Balouzat and the
414 zootechnicians at INSERM UMS006-CREFRE mouse facility ; the Blanchard and Robey teams for
415 help and discussions ; M.-F. Cesbron-Delauw for the anti-GRA1 and anti-GRA2 antibodies, H.
416 Acha-Orbea for the MutuDC, D. Buzoni-Gatel for the 76K parasites, S.-K. Kim, J. Boyle and J.
417 Boothroyd for the GFP⁺ Pru tachyzoites ; T. Hansen for the pL^d4 plasmid ; G. Schutz for the
418 B6.CamKII α -iCre mice ; I. Cebrian and D. Dunia for critical reading of the manuscript.

419 This work was supported by 'Institut National de la Santé et de la Recherche Médicale', IDEX
420 Toulouse 'Attractivity Chair' Program (to ER and NB), Human Frontier Science Program
421 Organization (CDA00047/2011 to NB), PIA PARAFRAP Consortium (ANR-11-LABX0024 to NB), PIA
422 ANINFIMIP equipment (ANR-11-EQPX-0003 to NB), Agence Nationale pour la Recherche (ANR-
423 18-CE15-0015 to NB and ES), 'Fondation pour la Recherche Médicale' to AS (FDT20170436953).

424 **Author Contributions**

425 Conceived and designed the experiments: AS, MB, ES, SB, EAR, NB. Performed the experiments:
426 AS, MB, ES, AL, EB, VCF, VV, SB. Analyzed the data: AS, MB, ES, AL, EB, VCF, VV, SB, RSL, EAR,
427 NB. Wrote the paper: NB with help of coauthors.

428 **Declaration of interests**

429 The authors declare no competing interests.

430

431 **Main Figure Titles and Legends**

432 **Figure 1. Expression of GRA6-OVA antigen by *T. gondii* leads to efficient parasite control and**
433 **lower CNS inflammation**

434 **(a)** Schematics of GRA6-OVA and vacOVA antigenic constructs expressed in the Tomato⁺
435 Prugnaud (Pru) parental strain. GRA6-OVA: fusion protein between GRA6(II) and LEQLE-
436 SIINFEKL sequence, driven by the GRA6 promoter. vacOVA: fusion protein between SAG1ΔGPI
437 and amino acids [140-386] of OVA, which contain the LEQLE-SIINFEKL sequence, driven by the
438 tubulin promoter. Representative immunofluorescent images of a parasitophorous vacuole and
439 an *ex vivo* cyst to illustrate activity of both promoters in tachyzoites and bradyzoites. Red:
440 intrinsic Tomato fluorescence. Green: anti-SIINFEKL staining for GRA6-OVA, anti-full length OVA
441 staining for vacOVA. **(b)** Schematics of experimental infections in mice infected i.p. with either
442 of the 3 parasite strains. Analyses of brain parasite load and immunological status 3 weeks
443 post-infection. **(c, d)** Number of brain cysts enumerated microscopically (mean +/- SEM) in H-2^b
444 C57BL/6 mice **(c)** and H-2^k CBA mice **(d)**. **(e)** Flow cytometry gating strategy to analyze myeloid
445 cells in the CNS. **(f)** Analysis of inflammatory CD45^{hi} CD11b⁺ myeloid cells and resident CD45^{int}
446 CD11b⁺ ('microglia') cells. Numbers on the representative contour plots show the mean
447 percentage +/- SD of each subset out of single live Ly6G⁻ NK1.1⁻ cells. Graph shows the ratio
448 (mean +/- SEM) of CD45^{hi} over CD45^{int} cells. **(g)** Representative brain cortical sections from
449 uninfected and infected mice, stained for Iba1. Scale bar: 100 μm for 5X images, 25 μm for 20X
450 images **(h)** Analysis of Ly6C^{hi} inflammatory monocytes. Numbers on the representative contour
451 plots show the mean percentage +/- SD of Ly6C^{hi} cells out of single live Ly6G⁻ NK1.1⁻ CD45^{hi}
452 CD11b⁺ cells. Graph shows absolute numbers (mean +/- SEM). **(i)** Proportion of MHC II⁺ cells
453 (DC) among Ly6C^{hi} monocytes (mean percentage +/- SD). **(j)** IFNγ production by CNS-isolated
454 CD4 T cells after incubation with brefeldin A. Numbers on the representative contour plots
455 show the mean percentage +/- SD of IFNγ⁺ out of CD4⁺ T cells. Graph shows absolute numbers
456 (mean +/- SEM). N = 4-8 mice / group. **(c, j)** Two experiments pooled. **(d)** Three experiments
457 pooled. **(f, h, i)** One experiment representative of 3 independent experiments. **(g)**
458 Representative field of view taken from a brain per condition. See also Figure S1.

459

460 **Figure 2. CD8 T cell responses against GRA6-OVA antigen are comparable whether or not**
461 **bradyzoites express the antigen**

462 **(a)** Schematics of the antigenic constructs introduced in GFP⁺ Prugnaud strain (*Tg.GFP*). GRA6-
463 OVA is driven either by the GRA6 promoter, active at the tachyzoite and bradyzoite stages, or by
464 the tachyzoite-restricted SAG1 promoter. **(b)** Immunofluorescence staining of *ex vivo*-isolated
465 cysts from CBA brains. Green: intrinsic parasite fluorescence and lectin-stained cyst wall. Red:
466 GRA6-OVA detected with anti-SIINFEKL antibody. Blue: GRA2. Scale bar 10 μ m. Right panel:
467 quantification of SIINFEKL fluorescence within cyst. Each dot represents one cyst. **(c)** MHC I K^b
468 presentation of GRA6-OVA-derived SIINFEKL peptide by MutuDC infected with the indicated
469 parasite lines, assessed by absorbance measurements following incubation with LacZ-inducible
470 OVA-specific B3Z CD8 T cell hybridomas. **(d)** Schematics of experimental infections in C57BL/6
471 mice infected i.p. with either of the 3 parasite strains. Evaluation of CD8 T cell responses 2
472 months post-infection. **(e-j)** IFN γ -producing CD8 T cells from spleen **(e, f, g)** or brain **(h, i, j)**
473 following *in vitro* restimulation with OVA-derived SIINFEKL peptide **(f, i)** and Tgd057-derived
474 SVLAFRRRL peptide **(g, j)**. **(e, h)** Numbers on the representative contour plots show the mean
475 percentage +/- SD of IFN γ ⁺ cells out of CD8⁺ T cells. **(f, g, i, j)** Absolute numbers (mean +/- SEM)
476 of IFN γ ⁺ CD8⁺ T cells. N = 5 mice / group. Representative of two independent experiments. See
477 also Figure S2.

478

479 **Figure 3. Tachyzoite-restricted GRA6-OVA antigen confers sustained parasite control and**
480 **protection against *T. gondii* encephalitis**

481 **(a)** Schematics of experimental infections in C57BL/6 mice infected i.p. with either of the 3
482 parasite strains. Analyses of brain parasite load and immune infiltrates 2 months post-infection.
483 **(b)** Brain cysts enumerated microscopically in infected C57BL/6 mice (mean +/- SEM). **(c, d)**
484 Parasite burden measured by qPCR on genomic DNA from infected C57BL/6 **(c)** or CBA **(d)** brains
485 (mean +/- SEM). **(e, f)** Analysis of inflammatory CD45^{hi} CD11b⁺ myeloid cells and resident

486 CD45^{int} CD11b⁺ ('microglia') cells. Numbers on the representative contour plots show the mean
487 percentage +/- SEM of each subset out of single live Ly6G⁻ NK1.1⁻ cells. Graphs show the
488 number of CD45^{int} CD11b⁺ microglia (mean +/- SEM) **(e)** or the ratio of CD45^{hi} over CD45^{int} cells
489 (mean +/- SEM) **(f)**. **(g, h)** Expression level of MHC II **(g)** and CD86 **(h)** on the surface of
490 microglia. Numbers on the representative histograms show the geomean +/- SD. Graphs
491 display the fold-increase of each marker with respect to microglia from uninfected mice (mean
492 +/- SEM). **(i)** Analysis of Ly6C^{hi} inflammatory monocytes. Numbers on the representative
493 contour plots show the mean percentage +/- SD of Ly6C^{hi} cells out of single live Ly6G⁻ NK1.1⁻
494 CD45^{hi} CD11b⁺ cells. Graph shows absolute numbers (mean +/- SEM). **(j)** Expression level of
495 CD86 on the surface of Ly6C^{hi} monocytes. Numbers on the representative histograms show the
496 geomean +/- SD. Graph displays the fold-increase over uninfected (mean +/- SEM). **(k)**
497 Proportion of MHC II⁺ cells (DC) among Ly6C^{hi} monocytes. Numbers on the representative
498 histograms and the graph show mean percentages +/- SD. **(l)** IFN γ production by CNS-infiltrating
499 CD4 T cells after incubation with brefeldin A. Numbers on the representative contour plots
500 show the mean percentage of IFN γ ⁺ out of CD4⁺ T cells +/- SD. Graph shows absolute numbers
501 (mean +/- SEM). For all panels, N = 9 mice / group with 2 experiments pooled, except for **(l)**
502 where N = 5 mice / group from one experiment.

503

504 **Figure 4. Defective control of vacOVA-expressing *T. gondii* is not due to improper**
505 **mobilization and effector differentiation of CD8 T cells in CNS**

506 **(a)** Schematics of experimental infections in C57BL/6 mice infected i.p. with either of the 3
507 parasite strains. Evaluation of CD8 T cell responses in spleen and brain 3 weeks post-infection.
508 **(b, d)** K^b-SIINFEKL dextramer labeling of spleen **(b)** and brain-infiltrating **(d)** CD8 T cells.
509 Numbers on the representative contour plots show the mean percentage of dextramer⁺ out of
510 CD8⁺ T cells +/- SD. Graph shows mean +/- SEM of absolute numbers. **(c, e)** Absolute numbers
511 of IFN γ -producing CD8 T cells from spleen **(c)** and brain **(e)** following *in vitro* restimulation with
512 OVA-derived SIINFEKL peptide (mean +/- SEM). **(f)** Analysis of triple-producing IFN γ ⁺ TNF⁺
513 granzyme B⁺ brain CD8 T cells after restimulation with SIINFEKL peptide. Numbers on the
21

514 representative contour plots show mean percentage of TNF⁺ granzyme B⁺ out of IFN γ ⁺ CD8 T
515 cells +/- SD. Graph shows absolute numbers of triple-producing CD8 T cells (mean +/- SEM).
516 N=5 mice/ group. **(b, c, d, e)** Representative of 4 independent experiments. **(f)** Representative
517 of 3 independent experiments.

518

519 **Figure 5. Poorer K^b-SIINFEKL presentation by neurons infected with *T. gondii* expressing**
520 **vacOVA compared to neurons infected with *T. gondii* expressing GRA6-OVA**

521 **(a)** Timeline of antigen presentation assay with *Tg*-infected primary neuronal cultures. AraC
522 was added to inhibit growth of glial cells. **(b, c)** Tropism and infection rate of the two Tomato⁺
523 parasites following co-staining with MAP2 (green) and GFAP (blue). Pictures represent
524 maximum intensity projections. Out of 24 fields, no vacuole was detected in a glial cell. Scale
525 bar 10 μ m. **(d)** K^b-SIINFEKL presentation by primary neurons infected for 24 h with the
526 indicated tachyzoites, assessed by absorbance measurements following incubation with
527 SIINFEKL-specific LacZ-inducible B3Z CD8 T cell hybridomas. **(b, c, d)** Representative of 2
528 independent experiments. See also Figure S3.

529

530 **Figure 6. MHC I presentation by CNS neurons is required for efficient brain control of *T. gondii***
531 **at chronic phase**

532 **(a)** Schematic representation of the L^dLox DNA cassette introduced in C57BL/6 fertilized eggs to
533 generate the B6.L^dLox mice. The cassette is a 12-kb genomic sequence comprising the L^d gene
534 modified with 2 LoxP sites flanking exons 1 to 3 (domains L, N and C1 according to
535 nomenclature from (Evans et al., 1982)) and the endogenous 5' and 3' UTR regulatory
536 sequences from BALB/c. **(b, c)** Flow cytometry labeling of H-2 K^b **(b)** and H-2 L^d **(c)** on the
537 surface of CD19⁻ CD3⁺ T cells, CD3⁻ CD19⁺ B cells and CD3⁻ CD19⁻ CD11c⁺ DC in the spleen of the
538 indicated mouse strains. Numbers on the histograms show the geometric mean +/- SD. **(b, c)**
539 Representative of two independent experiments. N=2-4 mice / group. **(d)** Schematics of
540 experimental infections in C57BL/6, B6.L^dLox and congenic B6.H-2^d mice infected i.p. with

541 *Tg.pTUB/vacOVA*, which naturally expresses GRA6. Evaluation of CD8 T cell responses and
542 parasite load 3 weeks later. **(e, f)** Absolute numbers of IFN γ -producing CD8 T cells isolated from
543 spleen **(e)** and brain **(f)**, following *in vitro* restimulation with L^d-restricted GRA6-derived HF10
544 peptide (mean +/- SEM). **(g)** Number of brain cysts in mice of the indicated genotypes (mean +/-
545 SEM). **(e-g)** Two experiments pooled with N=3-4 mice / group. **(h)** Schematics of the breeding
546 strategy and outcome in terms of MHC I molecules expressed by neurons vs. non-neuronal cells
547 in Cre⁻ and Cre⁺ mice. **(i)** Schematics of experimental infections in C57BL/6, B6.L^dLox.Cre⁺ or Cre⁻
548 infected *per os* with 15 cysts of the 76K strain. Evaluation of CD8 T cell responses and brain
549 parasite load 3 weeks later. **(j)** Number of brain cysts enumerated microscopically. **(k)** Brain
550 parasite burden measured by qPCR on genomic DNA. **(l)** Absolute number of total CD8 T cells
551 isolated from infected brains. **(m)** Absolute numbers of brain-isolated IFN γ -producing CD8 T
552 cells, following *in vitro* restimulation with L^d-restricted GRA6-derived HF10 peptide. **(j-m)**
553 Graphs show the mean +/- SEM. N=5-6 mice / group. Representative of 2 independent
554 experiments. See also Figure S4, S5 and S6.

555

556 KEY RESOURCES TABLE

REAGENT or RESOURCE	SOURCE	IDENTIFIER
Antibodies		
LEAF™ Purified anti-mouse CD16/32 antibody	BioLegend	Cat# 101321, RRID:AB_1877064
PE Rat Anti-Mouse CD8a	Thermo Fisher Scientific	Clone 53-6.7; Cat# 12-0081-83; RRID:AB_465531
BV421 Rat Anti-Mouse CD8a	BD Biosciences	Clone 53-6.7; Cat# 563898; RRID:AB_2738474
BV510 Rat Anti-Mouse CD4	BD Biosciences	Clone RM4-5; Cat# 563106; RRID:AB_2687550
PE-Cy™7 Rat Anti-Mouse CD4	BD Biosciences	Clone RM4-5 ; Cat# 552775; RRID:AB_394461
APC Rat Anti-Mouse IFN-γ	BD Biosciences	Clone XMG1.2; Cat# 554413; RRID:AB_398551
Alexa Fluor® 700 Rat anti-Mouse TNF	BD Biosciences	Clone MP6-XT22; Cat # 558000; RRID:AB_396980
PE Rat anti-mouse Granzyme B Monoclonal Antibody, eBioscience™	Thermo Fisher Scientific	Clone NGZB; Cat # 12-8898-82; RRID:AB_10870787
BV421 Hamster Anti-Mouse CD3e	BD Biosciences	Clone 145-2C11; Cat # 562600; RRID:AB_11153670
PE-Cy™7 Rat Anti-Mouse CD19	BD Biosciences	Clone 1D3; Cat # 552854; RRID:AB_394495
PE Hamster Anti-Mouse CD11c	BD Biosciences	Clone HL3; Cat # 557401; RRID:AB_396684
PE-CF594 Rat Anti-CD11b	BD Biosciences	Clone M1/70; Cat # 562287; RRID:AB_11154216
PerCP-Cy5.5 mouse anti-mouse H-2K ^b Antibody	Biolegend	Clone AF6-88.5; Cat # 116516; RRID:AB_1967133
Alexa Fluor® 700 Rat Anti-Mouse CD4	BD Biosciences	Clone RM4-5; Cat # 557956; RRID:AB_396956
Brilliant Violet 510™ Rat anti-mouse Ly-6G	BioLegend	clone 1A8; Cat # 127633; RRID:AB_2562937
PerCP-Cy™5.5 Rat Anti-Mouse CD45	BD Biosciences	Clone 30-F11; Cat # 550994; RRID:AB_394003
PE Mouse Anti-Mouse NK-1.1	BD Biosciences	Clone PK136; Cat# 557391; RRID:AB_396674
Alexa Fluor® 700 rat anti-mouse CCR2	R & D Systems	Clone # 475301; Cat # FAB5538N; RRID:AB_2725739
APC Rat anti-Mouse CD86	BD Biosciences	clone GL1; Cat # 558703; RRID:AB_2075114
Brilliant Violet 711™ Rat anti-mouse Ly-6C	BioLegend	clone HK1.4; Cat # 128037; RRID:AB_2562630
PE Rat Anti-CD11b	BD Biosciences	Clone M1/70; Cat # 553311; RRID:AB_394775
Alexa Fluor 700 rat anti-mouse CD86	BD Biosciences	Clone GL1; Cat # 560581; RRID:AB_1727517
FITC Rat Anti-Mouse I-A/I-E	BD Biosciences	Clone 2G9; Cat # 553623; RRID:AB_394958

FITC Hamster anti-mouse CD3	BD Biosciences	Clone 145-2C11; Cat # 553062; RRID:AB_394595
Monoclonal Anti-MAP2 (2a+2b) antibody produced in mouse	Sigma-Aldrich	clone AP-20; Cat # M1406; RRID:AB_477171
Anti-Glial Fibrillary Acidic Protein (GFAP) antibody	Millipore	Cat # AB5804; RRID:AB_2109645
Goat anti-Mouse IgG (H+L) Cross-Adsorbed Secondary Antibody, Alexa Fluor 488	Invitrogen	Cat # A-11001; RRID:AB_2534069
Goat anti-Rabbit IgG (H+L) Cross-Adsorbed Secondary Antibody, Alexa Fluor 647	Invitrogen	Cat # A-21244; RRID:AB_2535812
Goat anti-Mouse IgG (H+L) Highly Cross-Adsorbed Secondary Antibody, Alexa Fluor 594	Invitrogen	Cat # A-11032; RRID:AB_2534091
F(ab') ₂ -Goat anti-Rabbit IgG (H+L) Cross-Adsorbed Secondary Antibody, Alexa Fluor 488	Invitrogen	Cat # A-11070; RRID:AB_2534114
Goat anti-Rabbit IgG (H+L) Highly Cross-Adsorbed Secondary Antibody, Alexa Fluor 555	Invitrogen	Cat # A21429; RRID:AB_2535850
Goat anti-Mouse IgG (H+L) Cross-Adsorbed Secondary Antibody, Alexa Fluor 647	Invitrogen	Cat # A-21235; RRID: AB_2535804
Anti-Rabbit IgG (H+L), HRP Conjugate antibody	Promega	Cat # W4011; RRID:AB_430833
Anti-Mouse IgG (H+L) Antibody, HRP Conjugated	Promega	Cat # W4021; RRID:AB_430834
Rabbit anti-HPGSVNEFDF	(Buailon et al., 2017)	N/A
Rabbit anti-SIINFEKL	Biotem, this study	N/A
Mouse anti-GRA 1	Biotem; M.-F. Cesbron-Delauw	clone TG17.43
Mouse anti-GRA2	Biotem; M.-F. Cesbron-Delauw	clone Tg17-179
H2-K ^b -SIINFEKL Dextramer PE	Immudex	Cat # JD2163
Rabbit anti-TgProfilin	D. Soldati-Favre	PRF556
Rabbit anti-chicken OVA	Sigma	Cat # C6534; RRID: AB_258953
Rabbit anti-Iba1	Wako	Cat # 019-19741; RRID: AB_839504
Rabbit anti-MAP2	Millipore	Cat# AB5622; RRID: AB_91939
anti-H-2L ^d AF647	Biotem, (Ozato et al., 1980)	clone 30-5-7
Bacterial and Virus Strains		
Biological Samples		
Chemicals, Peptides, and Recombinant Proteins		
HPGSVNEFDF (HF10)	Genecust	N/A
SIINFEKL	Genecust	N/A
SVLAFRRL	Genecust	N/A
Mouse IFN- γ premium grade	Miltenyi Biotec	Cat # 130-105-774
Mycophenolic acid	Sigma-Aldrich	Cat # M5255
Xanthine	Sigma-Aldrich	Cat # X-2502
DNAse I from bovine pancreas	Sigma-Aldrich	Cat # DN25

Collagenase D from <i>Clostridium Histolyticum</i>	Roche	Cat # 11088882001
Rhodamine labeled Dolichos Biflorus Agglutinin (DBA)	Vector Laboratories	Cat # RL-1032; RRID: AB_2336396
eBioscience™ Fixable Viability Dye eFluor™ 450	Invitrogen	Cat # 65-0863-14
eBioscience™ Fixable Viability Dye eFluor™ 660	Invitrogen	Cat # 65-0864-14
LIVE/DEAD™ Fixable Green Dead Cell Stain Kit, for 488 nm excitation	Invitrogen	Cat # L34970
Triton X-100	Sigma-Aldrich	Cat # X100
Tween®20	Sigma-Aldrich	Cat # P1379
ProLong Diamond Anti-Fade Mounting medium with DAPI	Invitrogen	Cat # P36962
Paraformaldehyde 20 % aqueous solution	Electron Microscopy Sciences	Cat # 15713
Apicidin	Sigma-Aldrich	Cat # A8851
Laemmli Sample Buffer	BIO-RAD	Cat #1610737
Percoll	GE Healthcare	Cat # 17-0891-01
eBioscience Brefeldin A solution	Thermo Fisher Scientific	Cat # 00-4506-51
eBioscience Permeabilization Buffer (10X)	Thermo Fisher Scientific	Cat # 00-8333-56
Poly-D-lysine	Merck Millipore	Cat # A-003-E
UltraPure™ DNase/RNase-Free Distilled Water	Invitrogen	Cat # 10977035
Laminin Mouse Protein, Natural	Invitrogen	Cat # 23017-015
Papain	Worthington Biochemical Corporation	Cat # LK003176
Bovine Serum Albumin	Dutscher	Cat # SH30574.02
Trypsin Inhibitor from chicken egg white	Roche	Cat # 10109878001
B-27 supplement	Gibco	Cat # 17504044
GlutaMAX Supplement	Gibco	Cat # 35050061
Cytarabine Hydrochloride	Sigma-Aldrich	Cat # C6645
Normal Goat Serum	Vector Laboratories	Cat # S-1000
chlorophenol red-β-D-galactopyranoside CPRG	Roche	Cat # 10884308001
Glutaraldehyde 8% aqueous solution	Electron Microscopy Science	Cat # 16019
X-gal	Sigma-Aldrich	Cat # B4252
Potassium Ferrocyanide	Sigma-Aldrich	Cat # 60279
Potassium Ferricyanide	Sigma-Aldrich	Cat # 60299
Magnesium Chloride Hexahydrate	Sigma-Aldrich	Cat # M2670
Tetrodotoxin	Sigma-Aldrich	Cat # T8024
TBS	Euromedex	Cat # ET220
DAPI	Sigma-Aldrich	Cat # D9542
Fluoromount medium	Electron Microscopy Sciences	Cat # 17984-25
Critical Commercial Assays		

DNEasy Blood and Tissue Kit	Qiagen	Cat # 69504
Deposited Data		
Experimental Models: Cell Lines		
MutuDC	(Fuertes Marraco et al., 2012), H. Acha-Orbea	N/A
Human Foreskin Fibroblasts (HFF)	ATCC	Cat# SCRC-1041
SIINFEKL-specific LacZ-inducible CD8 T cell reporter hybridomas (B3Z)	(Karttunen et al., 1992), N. Shastri	N/A
Experimental Models: Organisms/Strains		
Mouse: CBA: CBA/JRj	Janvier	N/A
Mouse: B6 or C57BL/6: C57BL/6J	Janvier	N/A
Mouse: B6.H-2 ^d : B6.C-H2 ^d /bByJ	Jax	Cat # 000359
Mouse: B6.CamKII α -iCre	(Casanova et al., 2001), G. Schutz	N/A
Mouse: B6.L ^d Lox:	This study	N/A
<i>T. gondii</i> : 76K	(Bonnart et al., 2017); D. Buzoni-Gatel	N/A
<i>T. gondii</i> : Tg.Tomato: Pru. Δ hxgprt.tdTOMATO ^{prom TUB}	(Schaeffer et al., 2009)	N/A
<i>T. gondii</i> : Tg.pTUB/vacOVA: Pru. Δ hxgprt.tdTOMATO ^{prom TUB} .SAG1 Δ GPI-OVA _[140-386] ^{prom TUB/3'utr DHFR} +BLE	(Schaeffer et al., 2009)	N/A
<i>T. gondii</i> : Tg.pGRA6/GRA6-OVA: Pru. Δ hxgprt.tdTOMATO ^{prom TUB} .GRA6 _{II} -LEQLE-SIINFEKL ^{prom GRA6/3'utr GRA2} +HXGPRT	This study	N/A
<i>T. gondii</i> : Tg.GFP: Pru. Δ hxgprt.GFP ^{prom GRA1} .click beetle LUC ^{prom DHFR}	(Kim et al., 2007)	N/A
<i>T. gondii</i> : Tg.pGRA6/GRA6-OVA: Pru. Δ hxgprt.GFP ^{prom GRA1} .click beetle LUC ^{prom DHFR} .GRA6 _{II} -LEQLE-SIINFEKL ^{prom GRA6/3'utr GRA2} +HXGPRT	This study	N/A
<i>T. gondii</i> : Tg.pSAG1/GRA6-OVA: Pru. Δ hxgprt.GFP ^{prom GRA1} .click beetle LUC ^{prom DHFR} .GRA6 _{II} -LEQLE-SIINFEKL ^{prom SAG1/3'utr GRA2} +HXGPRT	This study	N/A
Oligonucleotides		
TOX9: 5'-AGGAGAGATATCAGGACTGTAG	(Feliu et al., 2013)	N/A
TOX11: 5'-GCGTCGTCTCGTCTAGATCG	(Feliu et al., 2013)	N/A
pri58-F: 5'-TTCCGAGCAGGTGACCTGGGTC	This study	N/A

pri92-R: 5'- CGTACGGGTACCATGGTTACAGTTTTTCAAAGTTGATTATACT CTCAAGCTGCTCAAGAAAATCAAACCTCATTCACTTCCCGG GT	This study	N/A
pri28F : 5'- CTAGATACCGTTCGTATAATGTATGCTATACGAAGTTATACTA GTGCTAGCATAACTTCGTATAATGTATGCTATACGAACGGTA T	This study	N/A
pri29R : 5'- CTAGATACCGTTCGTATAGCATACATTATACGAAGTTATGCTA GCACTAGTATAACTTCGTATAGCATACATTATACGAACGGTAT	This study	N/A
Recombinant DNA		
pL ^d 4	(Evans et al., 1982), T. Hansen	internal ID: NBpla93
pL ^d 4Lox	This study	internal ID: NBpla100
pGRA6/GRA6-OVA	This study	internal ID: NBpla119
pSAG1/GRA6-OVA	This study	internal ID NBpla190
Software and Algorithms		
ImageJ	NIH	N/A
FlowJo	TreeStar	N/A
Prism	GraphPad	N/A

558 **STAR Methods**

559 **CONTACT FOR REAGENT AND RESOURCE SHARING**

560 Further information and requests for resources and reagents should be directed to and will be
561 fulfilled by the Lead Contact, Nicolas Blanchard (nicolas.blanchard@inserm.fr)

562 **EXPERIMENTAL MODEL AND SUBJECT DETAILS**

563 **Human cell lines**

564 Human Foreskin Fibroblasts (HFF) were purchased from ATCC (see Key Resources Table). They
565 were maintained in DMEM supplemented with 10 % FCS (Gibco). Gender is unknown.

566 **Mouse cell lines and primary cells**

567 MutuDC, a C57BL/6-derived dendritic cell line, were obtained from H. Acha-Orbea (see Key
568 Resource Table) and grown using the recommended protocol, as in (Fuertes Marraco *et al.*,
569 2012). Bone marrow-derived DC from F1 C57BL/6 X B6.H-2^d (H-2^{bxd}) mice were generated as in
570 (Buillon *et al.*, 2017).

571 ***Toxoplasma gondii***

572 For all experiments, type II 76K or Prugnaud (Pru) derivatives (see Key Resource Table for
573 details) were used. Pru tachyzoites were maintained *in vitro* by serial passages on confluent
574 monolayers of HFF using DMEM supplemented with 1 % FCS (Gibco). 76K parasites were
575 passaged *in vivo* in CBA mice by *per os* inoculation of 100 cysts every 2-month. For intra-
576 peritoneal infections, infected HFF were scraped, tachyzoites were released through a 23G
577 needle, filtered through a 3 µm polycarbonate hydrophilic filter (it4ip S.A.) and 2-5x10²
578 tachyzoites were injected in 200 µl PBS. For *per os* infections, 200 µl of brain homogenate
579 containing 15 cysts was administered by oral gavage.

580 **Mice**

581 Animal care and use protocols were carried out under the control of the National Veterinary
582 Services and in accordance with the European regulations (EEC Council Directive, 2010/63/EU,
583 September 2010). Protocols inducing pain (CE no. 2015-02) were approved by the local Ethical
29

584 Committee for Animal Experimentation registered by the 'Comité National de Réflexion Ethique
585 sur l'Expérimentation Animale' under no. CEEA122. CBA/JRj and C57BL/6J (B6) mice were
586 purchased from Janvier (France). B6.C-H2^d/bByJ, abbreviated as B6.H-2^d, were purchased from
587 Jackson Laboratories (Bar Harbor, ME, USA). F1 C57BL/6 X B6.H-2^d (H-2^{bx^d}) were bred for this
588 study. B6.CamKII α -iCre were a gift from G. Schutz (Casanova et al., 2001). B6.L^dLox were
589 generated by additive transgenesis following microinjection of a linearized DNA cassette
590 containing a floxed H-2L^d allele into the pronucleus of C57BL/6J fertilized eggs. The floxed L^d
591 gene with two LoxP sites flanking exons 1 to 3 was obtained after modification of the pL^d4
592 plasmid that harbors a 12-kb BALB/c-derived genomic sequence (Evans et al., 1982). More
593 details on the pL^d4Lox plasmid construction are shown below. All mice were housed and bred
594 under specific pathogen-free conditions at the 'Centre Régional d'Exploration Fonctionnelle et
595 de Ressources Expérimentales' (CREFRE-Inserm UMS006). Age of mice used in experiments was
596 8-20 weeks. Mice used in experiments were males. Mice in B6.L^dLox.CamK-Cre^{+/-} experiments
597 were littermates. Number of mice and experimental replicates are indicated in the respective
598 figure legends.

599 **METHOD DETAILS**

600 **Generation of transgenic parasites**

601 Hxgprt-deficient GFP⁺ (Kim et al., 2007) and tdTomato⁺ Pru (Schaeffer et al., 2009) were used as
602 parental strains. Tachyzoites were transfected with plasmids encoding the GRA6_{II} open-reading
603 frame in frame with nucleotides encoding LEQLE-SIINFEKL, yielding the GRA6-OVA antigenic
604 construct. GRA6-OVA was flanked by *gra2* 3' UTR and by either the endogenous *gra6* promoter
605 and 5' UTR (pGRA6/GRA6-OVA) or the by the *sag1* promoter and 5'UTR (pSAG1/GRA6-OVA).
606 Plasmids were generated by a combination of DNA fragment synthesis (GeneArt, Thermo Fisher)
607 and standard cloning procedures and verified by sequencing. Parasite transfections were
608 performed as previously described (Feliu et al., 2013). In brief, 2x10⁷ freshly egressed
609 tachyzoites were electroporated with 50 μ g of NotI (New England Biolabs)-linearized plasmid
610 DNA. After selection in culture medium supplemented with mycophenolic acid (Sigma, 25

611 $\mu\text{g/ml}$) and xanthine (Sigma, 50 $\mu\text{g/ml}$), resistant tachyzoites were cloned by limiting dilution in
612 flat-bottom 96-well plates and presence of the transgene was verified by PCR and sequencing.

613 **Bradyzoite differentiation and Western blot**

614 For *in vitro* bradyzoite differentiation assays, HFF were seeded in 6-W plates and infected with
615 10^6 tachyzoites. After 24 h, the medium was replaced and supplemented with 40 nM of the
616 histone deacetylase inhibitor apicidin (Sigma-Aldrich) in order to promote bradyzoite
617 differentiation (Bougdour *et al.*, 2009; Boyle *et al.*, 2006). After 24 h for the untreated or 72 h
618 for the apicidin-treated, parasites were released with a 23-G needle, lysed in 1x Laemmli buffer
619 (Bio-Rad) containing 10 % 2-mercaptoethanol (Bio-Rad) and heated for 5 min at 70°C. Total cell
620 lysates were forced through a 29-G needle, separated by electrophoresis on 15 %
621 polyacrylamide gels and transferred to nitrocellulose membranes. Immunologic detection was
622 performed using purified rabbit anti-SIINFEKL antisera (custom-made, Biotem, Grenoble) and
623 mouse anti-GRA1 (Biotem) followed by horseradish peroxidase-conjugated antibodies
624 (Promega). Peroxidase activity was visualized by chemiluminescence and quantified using a
625 ChemiDoc XRS+ system (Bio-Rad).

626 **Isolation of spleen and brain leukocytes**

627 Spleens and brains were dissociated in complete RPMI (Gibco) supplemented with 10 % vol/vol
628 FCS (Gibco). Splenocytes were mashed through a 100 μm cell strainer (Falcon). Brains were
629 homogenized using a Potter, minced and digested for 45 min in RPMI containing 1 mg/ml
630 collagenase (Roche) and 0.1 mg/ml DNase (Sigma-Aldrich). Samples were then centrifuged at
631 600 g and suspended in 60 % (vol/vol) Percoll (GE Healthcare). A 30 % (vol/vol) Percoll solution
632 was overlaid and the tubes were centrifuged at 1000 g for 20 min. Brain leukocytes were
633 recovered from the interface. In both cases, erythrocytes were lysed using ACK buffer (100 μM
634 EDTA, 160 mM NH_4Cl and 10 mM NaHCO_3).

635 ***Ex vivo* T cell stimulation**

636 One-fifth of Percoll-isolated brain leukocytes or 10^6 splenocytes were incubated for 4 h 15 min
637 at 37°C in the presence of brefeldin A (eBioscience) with 10^5 bone marrow-derived DC from F1

638 C57BL/6 X B6.H-2^d (H-2^{bxd}) mice or with C57BL/6-derived MutuDC (Fuertes Marraco *et al.*,
639 2012), plus 200 nM of the following peptides as indicated in the legends: GRA6-derived
640 HPGSVNEFDF (HF10) presented by H-2L^d, OVA-derived SIINFEKL presented by H-2K^b and Tgd057-
641 derived SVLAFRRL presented by H-2K^b.

642 **Flow cytometry**

643 Following Fc receptor saturation (Biolegend) and dead cell detection with AF488 Live Dead/Cell
644 marker (Invitrogen) in PBS, cell suspensions were surface labelled with CD8α BV421 (53-6.7,
645 1/300, BD Pharmingen) or CD8α PE (53-6.7, 1/300, eBioscience), CD4 BV510 (RM4-5, 1/200, BD
646 Horizon) or CD4 Pe-Cy7 (RM4-5, 1/300, BD Pharmingen). Intracellular IFNγ (IFNγ-APC or AF700,
647 XMG1.2 1/300, BD Pharmingen), TNFα (TNFα AF700, MP6-XT22, 1/300, BD Pharmingen),
648 Granzyme B (Granzyme B PE, NGZB, 1/200, eBioscience) were detected after fixation in 4 %
649 paraformaldehyde solution (PFA, Electron Microscopy Sciences) and permeabilization with the
650 Permeabilization Buffer kit (eBioscience).

651 For *ex vivo* MHC I labeling, 10⁶ splenocytes were stained with FcR block and AF488 Live/Dead
652 cell marker in PBS. They were labelled with CD3 BV421 (145-2C1, 1/300, BD Horizon) or CD3
653 FITC (145-2C1, 1/300, BD Pharmingen), CD19 Pe-Cy7 (1D3,1/400, BD Pharmingen), CD11c PE
654 (N418, 1/300, eBioscience), CD11b PE-CF594 (M1/70, 1/3000, BD Horizon) or CD11b PE (M1/70,
655 1/400, BD Pharmingen), anti-H-2L^d AF647 (30-5-7, 1/100, Biotem) or anti-H-2K^b PerCP-Cy5.5
656 (AF6-88.5, 1/300, Biolegend). Samples were fixed using 4% PFA.

657 For *ex vivo* K^b-SIINFEKL dextramer analysis, splenocytes and brain leukocytes were incubated 1 h
658 at 37 °C with a solution of dextramer H-2 K^b-SL8 PE (1/50, Immudex). Cells were stained with
659 FcR block and eFluor 660 Fixable Viability Dye (1/1000, eBioscience) in PBS and then labelled
660 with CD8α BV421 (53-6.7, 1/300, BD Horizon) and CD4 AF700 (RM4-5, 1/200, BD Pharmingen)
661 or CD4 BV510 (RM4-5, 1/200, BD Horizon).

662 To analyze the phenotype and activation of CNS-isolated myeloid cells, brain leukocytes were
663 stained with FcR block and eFluor 450 Fixable Viability Dye (1/1000, eBioscience) in PBS and
664 then labelled using the following antibodies: Ly6G BV510 (1/200, 1A8, Biolegend), CD45 PerCP-

665 Cy5.5 (30-f 11, 1/300, BD Pharmingen), CD11b PE-CF594 (M1/70, 1/3000, BD Horizon), NK1.1 PE
666 (PK 136, 1/400, BD), CCR2 AF700 (FAB5538N, 1/200, R&D Systems), CD86 APC (GL1,1/300, BD
667 Pharmingen) or CD86 Alexa Fluor 700 (GL1, 1/500, BD Pharmingen), Ly6C BV711 (HK1.4, 1/1800,
668 Biolegend), MHC II I-A/I-E FITC (2G9, 1/300, BD Pharmingen). In all cases, samples were
669 ultimately fixed in 4 % PFA before acquisition on a BD Fortessa and analyzed using FlowJo (Tree
670 Star).

671 **Parasite load analysis**

672 For cyst enumeration, 5 % of total brain homogenate was labeled with rhodamine or
673 fluorescein-conjugated *Dolichos Biflorus* Agglutinin (Vector Laboratories). Cysts were counted
674 using an inverted fluorescence microscope. Quantification of parasite DNA by qPCR was
675 performed on genomic DNA extracted from 5 % of each brain homogenate, 10⁶ splenocytes or
676 5x10⁵ peritoneal exudate cells using the DNEasy Blood & Tissue Kit (Qiagen). As described
677 earlier (Feliu *et al.*, 2013), a 529-bp repeat element in the *T. gondii* genome was amplified using
678 the TOX9 and TOX11 primers (sequences shown in Key Resource Table). The number of parasite
679 genome per µg of tissue DNA was estimated by comparison with a standard curve, established
680 with a known number of Pru tachyzoites.

681 **IF labeling of *ex vivo* cysts**

682 Five percent of the brain homogenate was stained with rhodamine-conjugated DBA lectin, fixed
683 in 4% PFA for 10 min at room temperature (RT) and permeabilized in PBS - 0.2% Triton™ X100
684 (Sigma-Aldrich). Samples were then incubated with a custom-made rabbit anti-SIINFEKL (1/300,
685 Biotem) or anti-OVA (1/500, Sigma) and a mouse anti-GRA2 (1/3000, Biotem) diluted in PBS BSA
686 3 % (Dutscher), followed by incubation with AF555-coupled anti-rabbit Immunoglobulin G (IgG)
687 or AF488-coupled anti-rabbit (1/500) and AF647-coupled anti-mouse IgG (1/500, Life
688 Technologies, Thermo Fisher) diluted in PBS-BSA 3 %. Samples were mounted using ProLong™
689 Diamond Anti-Fade containing DAPI (Life Technologies, Thermo Fisher scientific) and imaged
690 using a Zeiss LSM710 confocal microscope. Quantifications of the GRA6-OVA signal were
691 performed using ImageJ software (NIH). Briefly, a filled mask encompassing the entire area of

692 the cyst was created based on the DBA lectin staining and the parasite fluorescence. The mean
693 intensity of the GRA6-OVA signal of masked pixels was measured and averaged from 3
694 equatorial planes for every individual cyst.

695 **IF labeling of HFF**

696 HFF were infected with Tg.pGRA6/GRA6-OVA or Tg.pTUB/vacOVA parasites during 24 h. After 2
697 washes in PBS, cells were fixed in PFA 4% for 20 min at RT and quenched in PBS glycine 100mM
698 (Sigma) for 10 min at RT. Cells were then washed in PBS and incubated with primary polyclonal
699 rabbit OVA (1/500, Sigma) or rabbit anti-SIINFELK (1/300, Biotem) in PBS-BSA 0,2%-saponin 0,05
700 %. After washing in the same buffer, cells were incubated with AF488-coupled anti-rabbit IgG
701 (1/500, Life Technologies). Coverslips were mounted using ProLong Diamond™ Anti-Fade
702 containing DAPI (Life Technologies, Thermo Fisher scientific). Images were acquired with a 63X
703 objective on a Zeiss LSM710 confocal microscope.

704 **Primary hippocampal neuronal cultures**

705 Primary neuronal cultures were derived from C57BL/6 embryonic day 17 hippocampi. One day
706 before dissection, flat-bottom 24-well plates with glass coverslips and flat-bottom 96-well plates
707 were coated with Poly-D-lysine (Merck) dissolved in Ultra-Pure™ Distilled Water (Gibco) to the
708 final concentration of 38,5 µg/ml. Coated plates were stored overnight at 37°C. The day of the
709 dissection, plates were washed twice with Ultra-Pure™ Distilled Water (Gibco) and coated with
710 laminin (mouse, 1/500, Invitrogen) during 3 h at 37°C. After dissection, hippocampi were
711 digested 8 min at 37°C with Papain solution (Worthington Biochemical Corp.) at 1 U/ml final
712 activity. Digestion was stopped using a solution composed of 1.5 mg/ml BSA (Dutscher),
713 1.5 mg/ml Trypsin inhibitor from chicken egg white (Sigma-Aldrich) and 66.7 µg/ml DNase
714 (Sigma-Aldrich) in PBS. Tissues were mechanically dissociated by trituration with a plastic
715 pipette, filtered through a 70 µm strainer (Falcon) and centrifuged at 210 g for 7 min. Cells were
716 suspended in Neurobasal®-A medium (Gibco) containing 2% B27® Supplement (vol/vol) (Gibco),
717 1% GlutaMAX™-I (vol/vol) (Gibco), 120 U/ml Penicillin, 120 µg/ml Streptomycin (Gibco) and
718 seeded at 2×10^5 cells per well for the 24-well plate and 4×10^4 cells per well for the 96-well

719 plate. Cells were then incubated at 37°C, 5% CO₂. At day 4 and 8, primary cultures were treated
720 with 5 µM of cytarabine hydrochloride (AraC) (Sigma-Aldrich) in order to inhibit growth of glial
721 cells. At day 11, 100 U/ml of mouse IFN γ (Miltenyi Biotec) was added. Twelve days after the
722 beginning of the culture, neurons were infected with *Tg.pGRA6/GRA6-OVA* or *Tg.pTUB/vacOVA*
723 strains. Respectively, 5x10⁴ or a serial dilution of 5x10⁴ to 2x10³ tachyzoites were added in
724 each well of the 24-well or 96-well plate. To assess L^d expression, hippocampal cultures were
725 established with B6.L^dLox.Cre+/- pups at postnatal day 1 using a similar procedure as above,
726 with the following modifications: 1,5x10⁵ cells were seeded per well in a 24 - well plate and
727 were not treated with AraC. At day 13, primary cultures were treated with mouse IFN γ
728 (0,5 µg/ml) and 1 µM Tetrodotoxin (TTX) (Sigma-Aldrich) as in (Chevalier *et al.*, 2011).

729 **IF labeling of primary neuronal cultures**

730 Twenty-four hours after infection, cells were fixed with 4 % PFA for 20 min at RT. After 2 x 5
731 min washes with PBS, cells were permeabilized with PBS - 0,05 % Triton™ X100 (Sigma-Aldrich)
732 for 5 min at RT. Following 3 x 5 min washes in PBS, non-specific binding sites were blocked with
733 PBS - 5 % Normal Goat Serum (NGS) (Vector Laboratories) - 0,05 % Tween®20 (Sigma-Aldrich)
734 for 1 h at RT. Cells were incubated overnight at 4°C with primary monoclonal mouse anti-
735 microtubule-associated protein 2 (MAP2, AP-20, 1/500, Sigma-Aldrich) and polyclonal rabbit
736 anti-glial fibrillary acidic protein (GFAP, 1/500, Merck) diluted in PBS - 3 % NGS - 0,05 %
737 Tween®20. Cells were washed 1 x 5 min with PBS, 3 x 5 min with PBS - 0,05 % Tween®20 and 5
738 min with PBS. Cells were incubated for 2 h at RT in presence of secondary antibodies AF488-
739 coupled anti-mouse immunoglobulin G (IgG) and AF647-coupled anti-rabbit IgG (Life
740 Technologies, Thermo Fisher) diluted in PBS - 3 % NGS - 0,05 % Tween®20 (1/500) and protected
741 from light. Samples were mounted using ProLong™ Diamond Anti-Fade with DAPI (Life
742 Technologies, Thermo Fisher). Z-stacks were acquired with a 63X objective on a Zeiss LSM710
743 confocal microscope and analyzed using ImageJ software. Extracellular H-2 L^d was stained with
744 1,2 µg/ml of mouse anti L^d (clone 30-5-7, Biotem) diluted in PBS-3 % NGS for 30 min on ice
745 followed by two washes with cold PBS. Steps of intracellular staining were the same as
746 described above except for the antibodies used. Cells were stained with a polyclonal rabbit

747 anti-microtubule-associated protein 2 (MAP2, 1/1000, Merck) or with a polyclonal rabbit anti-
748 glial fibrillary acidic protein (GFAP, 1/500, Merck), followed by both AF488-coupled anti-rabbit
749 IgG (1/500, Life Technologies, Thermo Fisher) and AF594-coupled anti-mouse IgG (1/500, Life
750 Technologies, Thermo Fisher). Quantification of L^d labeling was done with ImageJ. The intensity
751 of L^d labeling was recorded on multiple sections after applying a mask corresponding to the
752 MAP2⁺ or GFAP⁺ pixels.

753 **IF labeling of brain cortical floating sections**

754 After transcardial perfusion with NaCl 0,9 %, hemibrains were removed, fixed in 4 % PFA for
755 48 h at 4°C and washed in PBS for 5 min and 24 h at 4°C. Brains were transferred in PBS - 30 %
756 sucrose for 48 h at 4°C, sectioned coronally at 25 µm-thickness and stored in PBS - 30 %
757 ethylene glycol - 30 % glycerol at -20°C until processed further. For this, sections were washed 4
758 X 5 min in TBS (Euromedex), permeabilized with TBS - 0,1 % Triton™ X100 (Sigma-Aldrich) for
759 10 min at RT and rinsed once with TBS for 5 min. After antigen retrieval with TBS -
760 100 mM Tris - 12 mM EDTA - 0,05 % Tween®20 (Sigma-Aldrich) at pH 9 during 20 min at 100°C,
761 brain sections were washed 3 X 5 min in TBS. Non-specific binding sites were blocked with TBS -
762 5 % Normal Goat Serum (NGS) (Vector Laboratories) - 5 % BSA (Dutscher) - 0,1 % Tween®20 for
763 1 h at RT. Floating sections were incubated overnight at 4°C with rabbit anti-Iba1 (1/1000,
764 Wako) in TBS - 3 % NGS - 0,1 % Tween®20. Following several washes in TBS - 0,1 % Tween®20
765 and TBS, sections were incubated for 2 h at RT with secondary antibody AF647-coupled anti-
766 rabbit IgG (Thermo Fisher) diluted in TBS - 3 % NGS - 0,1 % Tween®20 (1/500) and protected
767 from light. Samples were washed alternatively in TBS - 0,1 % Tween®20 and TBS twice and
768 incubated with 1 µg/ml of DAPI (Sigma-Aldrich) in TBS for 30 min at RT. Sections were mounted
769 in Fluoromount medium (Electron Microscopy Sciences) after 2 washes in TBS. Images were
770 acquired with 5 X and 20 X objectives on Apotome Zeiss microscope and analyzed using ImageJ
771 software.

772 ***In vitro* antigen presentation assays**

773 Antigen presentation measurements with MutuDC were performed as described in (Buillon et
774 al., 2017). In brief, 5×10^4 MutuDC were seeded into flat-bottom 96-well plates and infected
775 for 24 h with serially diluted tachyzoites. The proportion of infected cells (i.e. GFP⁺ or Tomato⁺)
776 was controlled by flow cytometry. Presentation of the SIINFEKL peptide by K^b was assessed
777 following 16 h incubation at 37°C with 10^5 LacZ-inducible B3Z reporter hybridomas per well.
778 Production of β -galactosidase by the hybridomas was quantified using the chromogenic
779 substrate chlorophenol red- β -D-galactopyranoside (CPRG, Roche). Absorbance was read at 595
780 nm with a reference at 655 nm with a spectrophotometer (VersaMax, Molecular Devices).

781 For antigen presentation with primary neurons, 24 h after neuron infection, 10^5 B3Z reporter
782 hybridomas were seeded per well of the 96-well plate and incubated for 16 h at 37°C. After
783 fixation with 2 % PFA - 0,2 % glutaraldehyde (Electron Microscopy Sciences) for 20 min at RT and
784 2 x 5 min washes with PBS, cells were incubated with a solution containing 1 mg/ml 5-bromo-4-
785 chloro-3-indolyl- β -D-galactopyranoside (X-gal, Sigma-Aldrich), 5 mM potassium ferrocyanide
786 (Sigma-Aldrich), 5 mM potassium ferricyanide (Sigma-Aldrich), 2 mM MgCl₂ (Sigma-Aldrich) in
787 PBS. X-gal-positive (blue) cells were counted microscopically with a 20X magnification. With
788 neurons, the X-gal assay was preferred over the bulk CPRG read-out because of its higher
789 sensitivity.

790 **Plasmids**

791 ***pGRA6/GRA6-OVA***

792 The pGRA6/GRA6-OVA plasmid was constructed by In-fusion (Takara) cloning of a GRA6(II)-
793 LEQLE-SIINFEKL insert (abbreviated as GRA6-OVA) into the 5' BstEII / 3' NcoI-linearized and gel
794 purified pGRA.HPT.GRA6(II) vector, a *T. gondii* expression vector containing a HXGPRT resistance
795 cassette (Feliu et al., 2013). The GRA6-OVA sequence was PCR-amplified from type II Pru
796 genomic DNA using a forward (pri58-F) and a reverse primer (pri92-R) (sequences shown in Key
797 Resource Table) in order to introduce the LEQLE-SIINFEKL coding sequence at the C-terminus of
798 GRA6(II) and to add extremities annealing with the ends of the linearized vector for the fusion
799 cloning. The resulting pGRA6/GRA6-OVA plasmid (internal ID NBpla119) contains the GRA6-

800 OVA coding sequence flanked by the endogenous GRA6(II) promoter/5'UTR and the 3'UTR from
801 GRA2(I) as well as the HXGPRT resistance cassette.

802 **pSAG1/GRA6-OVA**

803 To obtain the pSAG1/GRA6-OVA plasmid, the pGRA6/GRA6-OVA plasmid was modified to
804 replace the GRA6(II) promoter/5'UTR and GRA6-OVA coding sequence by a synthetic DNA
805 fragment containing the SAG1 promoter/5'UTR and GRA6-OVA coding sequence using 5'
806 HindIII/3' NcoI restriction cloning. The sequence of the introduced synthetic fragment is shown
807 below, with HindIII/NcoI sites underlined and GRA6-OVA ORF in bold:

808 AAGCTTTTACATCCGTTGCCTTTTCCACGGTCCGTGATTTTCATGTGCGTGCAGCTTCAAAGACTGGTCGT
809 GCGACTAATAAGACTGCAGTGACAGGTGCAATGGTGGGCACCTTGCTGATGACTATCTACTGCAAAGTC
810 TGAGACAACGAACGAACTTCCCACACGAGGCATTTGAACTGACGGTGTCTAGGTAATATGCACTGCA
811 AGACACGGTACTGGGGCCTCGCTGAATTAGGGGCCGATCTCGTTGCCCTATCAGTGCTCACAGTGCCGC
812 AACGTAACACCAGGGCAGGTTCTTGACAGTGGCAACAATGTGCGACGGGCGTGTGAACGTTTCGTAGTC
813 ATAGCGCTAGCACGTACCTAGCCACATGGTCGTGAGGAGCTTTACCATGCGTCTAGAAGGTGGATGCGG
814 GACACGCCTTCTGGCCTTTGGCTCCCGAGACGCGTGTCTAACCACAAACCTTGAGACGCGTGTCCAA
815 CCACGCACCCTGACACGCGTGTCCAACCACGCACCCTGAGACGCGTGTCTAACCACGCACCCTGAGAC
816 GCGTGTCTAACCACGCACCCTGAGACGCGTGTCTGCCGCACAATGTGCACCTGTAGGAAGCTGTAGTC
817 ACTGCTGATTCTCACTGTTCTCGGCAAGGGCCGACGACCGGAGTACAGTTTTTGTGGGCAGAGCCGTTGT
818 GCAGCTTTCCGTTCTTCTCGGTTGTGTCACATGTGTCATTGTCGTGTAACACACGGTTGT**ATGGCACACG**
819 **GTGGCATCTATCTGAGGCAGAAGCGTAACTTCTGTCCTTAACTGTCTCCACAGTTGCTGTGGTCTTTGT**
820 **AGTCTTCATGGGTGTA**CTCGTCAATTCGTTGGGTGGAGTCGCTGTCGAGCAGACAGCGGTGGTGT**TA**
821 **GGCAGACCCCTTCGGAAACCGTTTCGAGCGGTGGACAGCAAGAAGCAGTGGGGACCACTGAAGACTA**
822 **TGTCAACTCTTCGGCGATGGGCGGTGGCCAAGGCGACTCGTTAGCTGAAGATGATAACAACCTCCGATG**
823 **CGGCGGAGGGCGACGTTGACCCTTTCCGCGCTGGCGAATGAGGGGAAGTCGGAGGCGCGTGGCCC**
824 **GTCGCTCGAGGAAAGAATCGAAGAACAGGGCACAAGACGACGTTACTCCTCTGTTCAAGAACCACAA**
825 **GCGAAGGTGCCTAGCAAACGAACACAGAAACGCCACAGACTCATTGGTGCTGTGGTGTGGCAGTATC**
826 **TGTGGCAATGCTTACCGCTTTCTTCTCGAAGGACTGGACGACGCTCTCCCAAGAACCATCTGGGGG**
827 **TGGTGGTGGAAATGATGCAGGCAATAATGCTGGGAACGGTGGGAATGAAGGCAGAGGTGAAGGAG**

Salvioni *et al.*

828 **GCGAGGATGACAGGCGCCCGTTGCACCCGGGAAGTGTGAATGAGTTTGATTTCTTGAGCAGCTTGAG**
829 **AGTATAATCAACTTTGAAAACTGTAA**CCATGG

830 The resulting pSAG1/GRA6-OVA plasmid (internal ID NBpla 190) contains the GRA6-OVA coding
831 sequence flanked by the SAG1 promoter/5'UTR and the 3'UTR from GRA2(I) as well as a HXGPRT
832 resistance cassette.

833 ***pL^d4Lox plasmid***

834 The pL^d4 plasmid (internal ID NBpla93, kind gift of T. Hansen) contains 12-kb of genomic
835 sequence of BALB/c H-2 L^d gene inserted into pBR327 backbone between EcoRI and HindIII
836 (Evans *et al.*, 1982).

837 A pair of reverse complement primers (pri28F and pri29R, see sequences in Key Resource Table)
838 were annealed *in vitro* in order to create two distinct LoxP sites (to make sure that
839 recombination is irreversible) flanked by cohesive ends that permit cloning into XbaI site. **SpeI**
840 and **NheI** restriction sites, which are compatible for religation with XbaI, were included between
841 the LoxP sites:

842 CTAGATACCGTTCGTATAATGTATGCTATACGAAGTTAT**ACTAGTGCTAGCATAACTTCGTATAATGTATG**
843 **CTATACGAACGGTAT**

844 The XbaI-digested annealed fragment was cloned into XbaI-linearized pUC19 to obtain pUC19 |
845 LoxP |SpeI |NheI | LoxP (internal ID NBpla95). A 1.6kb XbaI-excised fragment from pL^d4
846 containing the first 3 exons (L,N,C1 (Ozato *et al.*, 1983)) was cloned into NheI-linearized pUC19 |
847 LoxP |SpeI |NheI | LoxP to obtain pUC19 | LoxP | SpeI | L^d exons 1-3 | LoxP (internal ID
848 NBpla99).

849 The LoxP | SpeI | L^d exons 1-3 | LoxP fragment was then excised with XbaI and cloned into XbaI-
850 opened pL^d4 to obtain pL^d4Lox (internal ID NBpla100). Clones were confirmed by restriction
851 digest and sequencing.

852 **QUANTIFICATION AND STATISTICAL ANALYSIS**

Salvioni *et al.*

853 Statistical analyses for all experiments were performed with Prism software v7 (GraphPad). In
854 experiments comparing only two groups, non-parametric Mann-Whitney tests were used to
855 compare the experimental group with the control group. For other experiments including 3
856 groups, non-parametric ANOVA tests (Kruskal-Wallis with Dunn's correction for multiple tests)
857 were used. Individual P values are indicated on the figures.

858

859 **References**

- 860 Bernard-Valnet, R., Yshii, L., Queriaux, C., Nguyen, X.H., Arthaud, S., Rodrigues, M., Canivet,
861 A., Morel, A.L., Matthys, A., Bauer, J., *et al.* (2016). CD8 T cell-mediated killing of orexinergic
862 neurons induces a narcolepsy-like phenotype in mice. *Proc Natl Acad Sci U S A* *113*, 10956-
863 10961.
- 864 Bhadra, R., Cobb, D.A., and Khan, I.A. (2013). Donor CD8+ T cells prevent *Toxoplasma gondii*
865 de-encystation but fail to rescue the exhausted endogenous CD8+ T cell population. *Infect*
866 *Immun* *81*, 3414-3425.
- 867 Biswas, A., Bruder, D., Wolf, S.A., Jeron, A., Mack, M., Heimesaat, M.M., and Dunay, I.R.
868 (2015). Ly6C(high) monocytes control cerebral toxoplasmosis. *J Immunol* *194*, 3223-3235.
- 869 Biswas, A., French, T., Dusedau, H.P., Mueller, N., Riek-Burchardt, M., Dudeck, A., Bank, U.,
870 Schuler, T., and Dunay, I.R. (2017). Behavior of Neutrophil Granulocytes during *Toxoplasma*
871 *gondii* Infection in the Central Nervous System. *Frontiers in cellular and infection microbiology*
872 *7*, 259.
- 873 Blanchard, N., Dunay, I.R., and Schluter, D. (2015). Persistence of *Toxoplasma gondii* in the
874 central nervous system: a fine-tuned balance between the parasite, the brain and the immune
875 system. *Parasite Immunol* *37*, 150-158.
- 876 Blanchard, N., Gonzalez, F., Schaeffer, M., Joncker, N.T., Cheng, T., Shastri, A.J., Robey, E.A.,
877 and Shastri, N. (2008). Immunodominant, protective response to the parasite *Toxoplasma gondii*
878 requires antigen processing in the endoplasmic reticulum. *Nat Immunol* *9*, 937-944.
- 879 Bonnart, C., Feuillet, G., Vasseur, V., Cenac, N., Vergnolle, N., and Blanchard, N. (2017).
880 Protease-activated receptor 2 contributes to *Toxoplasma gondii*-mediated gut inflammation.
881 *Parasite Immunol* *39*.
- 882 Bougdour, A., Maubon, D., Baldacci, P., Ortet, P., Bastien, O., Bouillon, A., Barale, J.C.,
883 Pelloux, H., Menard, R., and Hakimi, M.A. (2009). Drug inhibition of HDAC3 and epigenetic
884 control of differentiation in Apicomplexa parasites. *J Exp Med* *206*, 953-966.
- 885 Boyle, J.P., Saeij, J.P., Cleary, M.D., and Boothroyd, J.C. (2006). Analysis of gene expression
886 during development: lessons from the Apicomplexa. *Microbes Infect* *8*, 1623-1630.
- 887 Brown, C.R., Hunter, C.A., Estes, R.G., Beckmann, E., Forman, J., David, C., Remington, J.S.,
888 and McLeod, R. (1995). Definitive identification of a gene that confers resistance against
889 *Toxoplasma* cyst burden and encephalitis. *Immunology* *85*, 419-428.
- 890 Buailon, C., Guerrero, N.A., Cebrian, I., Blanie, S., Lopez, J., Bassot, E., Vasseur, V., Santi-
891 Rocca, J., and Blanchard, N. (2017). MHC I presentation of *Toxoplasma gondii*
892 immunodominant antigen does not require Sec22b and is regulated by antigen orientation at the
893 vacuole membrane. *Eur J Immunol* *47*, 1160-1170.
- 894 Cabral, C.M., McGovern, K.E., MacDonald, W.R., Franco, J., and Koshy, A.A. (2017).
895 Dissecting Amyloid Beta Deposition Using Distinct Strains of the Neurotropic Parasite
896 *Toxoplasma gondii* as a Novel Tool. *ASN Neuro* *9*, 1759091417724915.
- 897 Cabral, C.M., Tuladhar, S., Dietrich, H.K., Nguyen, E., MacDonald, W.R., Trivedi, T., Devineni,
898 A., and Koshy, A.A. (2016). Neurons are the Primary Target Cell for the Brain-Tropic
899 Intracellular Parasite *Toxoplasma gondii*. *PLoS pathogens* *12*, e1005447.
- 900 Casanova, A., Blatche, M.C., Ferre, C.A., Martin, H., Gonzalez-Dunia, D., Nicu, L., and Larrieu,
901 G. (2018). Self-Aligned Functionalization Approach to Order Neuronal Networks at the Single-
902 Cell Level. *Langmuir : the ACS journal of surfaces and colloids* *34*, 6612-6620.

- 903 Casanova, E., Fehsenfeld, S., Mantamadiotis, T., Lemberger, T., Greiner, E., Stewart, A.F., and
 904 Schutz, G. (2001). A CamKIIalpha iCre BAC allows brain-specific gene inactivation. *Genesis* 31,
 905 37-42.
- 906 Cebrian, C., Zucca, F.A., Mauri, P., Steinbeck, J.A., Studer, L., Scherzer, C.R., Kanter, E.,
 907 Budhu, S., Mandelbaum, J., Vonsattel, J.P., *et al.* (2014). MHC-I expression renders
 908 catecholaminergic neurons susceptible to T-cell-mediated degeneration. *Nat Commun* 5, 3633.
- 909 Chevalier, G., Suberbielle, E., Monnet, C., Duplan, V., Martin-Blondel, G., Farrugia, F., Le
 910 Masson, G., Liblau, R., and Gonzalez-Dunia, D. (2011). Neurons are MHC class I-dependent
 911 targets for CD8 T cells upon neurotropic viral infection. *PLoS pathogens* 7, e1002393.
- 912 Chu, H.H., Chan, S.W., Gosling, J.P., Blanchard, N., Tsitsiklis, A., Lythe, G., Shastri, N.,
 913 Molina-Paris, C., and Robey, E.A. (2016). Continuous Effector CD8(+) T Cell Production in a
 914 Controlled Persistent Infection Is Sustained by a Proliferative Intermediate Population. *Immunity*
 915 45, 159-171.
- 916 Colonna, M., and Butovsky, O. (2017). Microglia Function in the Central Nervous System
 917 During Health and Neurodegeneration. *Annu Rev Immunol* 35, 441-468.
- 918 Corriveau, R.A., Huh, G.S., and Shatz, C.J. (1998). Regulation of class I MHC gene expression
 919 in the developing and mature CNS by neural activity. *Neuron* 21, 505-520.
- 920 Di Liberto, G., Pantelyushin, S., Kreutzfeldt, M., Page, N., Musardo, S., Coras, R., Steinbach, K.,
 921 Vincenti, I., Klimek, B., Lingner, T., *et al.* (2018). Neurons under T Cell Attack Coordinate
 922 Phagocyte-Mediated Synaptic Stripping. *Cell* 175, 458-471 e419.
- 923 Elmer, B.M., and McAllister, A.K. (2012). Major histocompatibility complex class I proteins in
 924 brain development and plasticity. *Trends in neurosciences* 35, 660-670.
- 925 Evans, G.A., Margulies, D.H., Shykind, B., Seidman, J.G., and Ozato, K. (1982). Exon shuffling:
 926 mapping polymorphic determinants on hybrid mouse transplantation antigens. *Nature* 300, 755-
 927 757.
- 928 Feliu, V., Vasseur, V., Grover, H.S., Chu, H.H., Brown, M.J., Wang, J., Boyle, J.P., Robey, E.A.,
 929 Shastri, N., and Blanchard, N. (2013). Location of the CD8 T Cell Epitope within the Antigenic
 930 Precursor Determines Immunogenicity and Protection against the *Toxoplasma gondii* Parasite.
 931 *PLoS pathogens* 9, e1003449.
- 932 Ferguson, D.J., and Hutchison, W.M. (1987). The host-parasite relationship of *Toxoplasma*
 933 *gondii* in the brains of chronically infected mice. *Virchows Archiv. A, Pathological anatomy and*
 934 *histopathology* 411, 39-43.
- 935 Fox, B.A., Falla, A., Rommereim, L.M., Tomita, T., Gigley, J.P., Mercier, C., Cesbron-Delauw,
 936 M.F., Weiss, L.M., and Bzik, D.J. (2011). Type II *Toxoplasma gondii* KU80 knockout strains
 937 enable functional analysis of genes required for cyst development and latent infection. *Eukaryot*
 938 *Cell* 10, 1193-1206.
- 939 Frickel, E.M., Sahoo, N., Hopp, J., Gubbels, M.J., Craver, M.P., Knoll, L.J., Ploegh, H.L., and
 940 Grotenbreg, G.M. (2008). Parasite stage-specific recognition of endogenous *Toxoplasma gondii*-
 941 derived CD8+ T cell epitopes. *The Journal of infectious diseases* 198, 1625-1633.
- 942 Fuertes Marraco, S.A., Grosjean, F., Duval, A., Rosa, M., Lavanchy, C., Ashok, D., Haller, S.,
 943 Otten, L.A., Steiner, Q.G., Descombes, P., *et al.* (2012). Novel murine dendritic cell lines: a
 944 powerful auxiliary tool for dendritic cell research. *Front Immunol* 3, 331.
- 945 Glynn, M.W., Elmer, B.M., Garay, P.A., Liu, X.B., Needleman, L.A., El-Sabeawy, F., and
 946 McAllister, A.K. (2011). MHCI negatively regulates synapse density during the establishment of
 947 cortical connections. *Nature neuroscience* 14, 442-451.

- 948 Guo, M., Mishra, A., Buchanan, R.L., Dubey, J.P., Hill, D.E., Gamble, H.R., Jones, J.L., and
 949 Pradhan, A.K. (2016). A Systematic Meta-Analysis of *Toxoplasma gondii* Prevalence in Food
 950 Animals in the United States. *Foodborne pathogens and disease* 13, 109-118.
- 951 Heneka, M.T., Carson, M.J., El Khoury, J., Landreth, G.E., Brosseron, F., Feinstein, D.L.,
 952 Jacobs, A.H., Wyss-Coray, T., Vitorica, J., Ransohoff, R.M., *et al.* (2015). Neuroinflammation in
 953 Alzheimer's disease. *Lancet Neurol* 14, 388-405.
- 954 Herz, J., Johnson, K.R., and McGavern, D.B. (2015). Therapeutic antiviral T cells
 955 noncytopathically clear persistently infected microglia after conversion into antigen-presenting
 956 cells. *Journal of Experimental Medicine* 212, 1153-1169.
- 957 Hidano, S., Randall, L.M., Dawson, L., Dietrich, H.K., Konradt, C., Klover, P.J., John, B., Harris,
 958 T.H., Fang, Q., Turek, B., *et al.* (2016). STAT1 Signaling in Astrocytes Is Essential for Control
 959 of Infection in the Central Nervous System. *MBio* 7.
- 960 Huh, G.S., Boulanger, L.M., Du, H., Riquelme, P.A., Brotz, T.M., and Shatz, C.J. (2000).
 961 Functional requirement for class I MHC in CNS development and plasticity. *Science* 290, 2155-
 962 2159.
- 963 Hwang, S., Cobb, D.A., Bhadra, R., Youngblood, B., and Khan, I.A. (2016). Blimp-1-mediated
 964 CD4 T cell exhaustion causes CD8 T cell dysfunction during chronic toxoplasmosis. *J Exp Med*
 965 213, 1799-1818.
- 966 John, B., Ricart, B., Tait Wojno, E.D., Harris, T.H., Randall, L.M., Christian, D.A., Gregg, B.,
 967 De Almeida, D.M., Weninger, W., Hammer, D.A., and Hunter, C.A. (2011). Analysis of behavior
 968 and trafficking of dendritic cells within the brain during toxoplasmic encephalitis. *PLoS*
 969 *pathogens* 7, e1002246.
- 970 Karttunen, J., Sanderson, S., and Shastri, N. (1992). Detection of rare antigen-presenting cells by
 971 the lacZ T-cell activation assay suggests an expression cloning strategy for T-cell antigens. *Proc*
 972 *Natl Acad Sci U S A* 89, 6020-6024.
- 973 Kim, S.K., Karasov, A., and Boothroyd, J.C. (2007). Bradyzoite-specific surface antigen SRS9
 974 plays a role in maintaining *Toxoplasma gondii* persistence in the brain and in host control of
 975 parasite replication in the intestine. *Infect Immun* 75, 1626-1634.
- 976 Klein, R.S., and Hunter, C.A. (2017). Protective and Pathological Immunity during Central
 977 Nervous System Infections. *Immunity* 46, 891-909.
- 978 Kreutzfeldt, M., Bergthaler, A., Fernandez, M., Bruck, W., Steinbach, K., Vorm, M., Coras, R.,
 979 Blumcke, I., Bonilla, W.V., Fleige, A., *et al.* (2013). Neuroprotective intervention by interferon-
 980 gamma blockade prevents CD8+ T cell-mediated dendrite and synapse loss. *J Exp Med* 210,
 981 2087-2103.
- 982 Malo, C.S., Huggins, M.A., Goddery, E.N., Tolcher, H.M.A., Renner, D.N., Jin, F., Hansen,
 983 M.J., Pease, L.R., Pavelko, K.D., and Johnson, A.J. (2018). Non-equivalent antigen presenting
 984 capabilities of dendritic cells and macrophages in generating brain-infiltrating CD8 (+) T cell
 985 responses. *Nat Commun* 9, 633.
- 986 McDole, J.R., Danzer, S.C., Pun, R.Y., Chen, Y., Johnson, H.L., Pirko, I., and Johnson, A.J.
 987 (2010). Rapid formation of extended processes and engagement of Theiler's virus-infected
 988 neurons by CNS-infiltrating CD8 T cells. *Am J Pathol* 177, 1823-1833.
- 989 McManus, R.M., and Heneka, M.T. (2017). Role of neuroinflammation in neurodegeneration:
 990 new insights. *Alzheimer's research & therapy* 9, 14.
- 991 Melzer, T.C., Cranston, H.J., Weiss, L.M., and Halonen, S.K. (2010). Host Cell Preference of
 992 *Toxoplasma gondii* Cysts in Murine Brain: A Confocal Study. *J Neuroparasitology* 1.

- 993 Meuth, S.G., Herrmann, A.M., Simon, O.J., Siffrin, V., Melzer, N., Bittner, S., Meuth, P.,
 994 Langer, H.F., Hallermann, S., Boldakowa, N., *et al.* (2009). Cytotoxic CD8+ T cell-neuron
 995 interactions: perforin-dependent electrical silencing precedes but is not causally linked to
 996 neuronal cell death. *The Journal of neuroscience : the official journal of the Society for*
 997 *Neuroscience* 29, 15397-15409.
- 998 Mohle, L., Israel, N., Paarmann, K., Krohn, M., Pietkiewicz, S., Muller, A., Lavrik, I.N.,
 999 Buguliskis, J.S., Schott, B.H., Schluter, D., *et al.* (2016). Chronic *Toxoplasma gondii* infection
 1000 enhances beta-amyloid phagocytosis and clearance by recruited monocytes. *Acta*
 1001 *neuropathologica communications* 4, 25.
- 1002 O'Brien, C.A., Batista, S.J., Still, K.M., and Harris, T.H. (2019). IL-10 and ICOS Differentially
 1003 Regulate T Cell Responses in the Brain during Chronic *Toxoplasma gondii* Infection. *J Immunol*
 1004 202, 1755-1766.
- 1005 O'Brien, C.A., Overall, C., Konradt, C., O'Hara Hall, A.C., Hayes, N.W., Wagage, S., John, B.,
 1006 Christian, D.A., Hunter, C.A., and Harris, T.H. (2017). CD11c-Expressing Cells Affect
 1007 Regulatory T Cell Behavior in the Meninges during Central Nervous System Infection. *J*
 1008 *Immunol* 198, 4054-4061.
- 1009 Ondounda, M., Ilozue, C., and Magne, C. (2016). Cerebro-meningeal infections in HIV-infected
 1010 patients: a study of 116 cases in Libreville, Gabon. *African health sciences* 16, 603-610.
- 1011 Ozato, K., Evans, G.A., Shykind, B., Margulies, D.H., and Seidman, J.G. (1983). Hybrid H-2
 1012 histocompatibility gene products assign domains recognized by alloreactive T cells. *Proc Natl*
 1013 *Acad Sci U S A* 80, 2040-2043.
- 1014 Ozato, K., Hansen, T.H., and Sachs, D.H. (1980). Monoclonal antibodies to mouse MHC
 1015 antigens. II. Antibodies to the H-2Ld antigen, the products of a third polymorphic locus of the
 1016 mouse major histocompatibility complex. *J Immunol* 125, 2473-2477.
- 1017 Pappas, G., Roussos, N., and Falagas, M.E. (2009). Toxoplasmosis snapshots: global status of
 1018 *Toxoplasma gondii* seroprevalence and implications for pregnancy and congenital toxoplasmosis.
 1019 *International journal for parasitology* 39, 1385-1394.
- 1020 Parlog, A., Harsan, L.A., Zagrebelsky, M., Weller, M., von Elverfeldt, D., Mawrin, C., Korte, M.,
 1021 and Dunay, I.R. (2014). Chronic murine toxoplasmosis is defined by subtle changes in neuronal
 1022 connectivity. *Disease models & mechanisms* 7, 459-469.
- 1023 Perry, C.E., Gale, S.D., Erickson, L., Wilson, E., Nielsen, B., Kauwe, J., and Hedges, D.W.
 1024 (2016). Seroprevalence and Serointensity of Latent *Toxoplasma gondii* in a Sample of Elderly
 1025 Adults With and Without Alzheimer Disease. *Alzheimer disease and associated disorders* 30,
 1026 123-126.
- 1027 Rall, G.F., Mucke, L., and Oldstone, M.B. (1995). Consequences of cytotoxic T lymphocyte
 1028 interaction with major histocompatibility complex class I-expressing neurons in vivo. *J Exp Med*
 1029 182, 1201-1212.
- 1030 Russo, M.V., and McGavern, D.B. (2015). Immune Surveillance of the CNS following Infection
 1031 and Injury. *Trends in immunology* 36, 637-650.
- 1032 Sa, Q., Ochiai, E., Tiwari, A., Perkins, S., Mullins, J., Gehman, M., Huckle, W., Eyestone, W.H.,
 1033 Saunders, T.L., Shelton, B.J., and Suzuki, Y. (2015). Cutting Edge: IFN-gamma Produced by
 1034 Brain-Resident Cells Is Crucial To Control Cerebral Infection with *Toxoplasma gondii*. *J*
 1035 *Immunol* 195, 796-800.

- 1036 Sauer, B.M., Schmalstieg, W.F., and Howe, C.L. (2013). Axons are injured by antigen-specific
1037 CD8(+) T cells through a MHC class I- and granzyme B-dependent mechanism. *Neurobiology of*
1038 *disease* 59, 194-205.
- 1039 Schaeffer, M., Han, S.J., Chtanova, T., van Dooren, G.G., Herzmark, P., Chen, Y., Roysam, B.,
1040 Striepen, B., and Robey, E.A. (2009). Dynamic imaging of T cell-parasite interactions in the
1041 brains of mice chronically infected with *Toxoplasma gondii*. *J Immunol* 182, 6379-6393.
- 1042 Stock, A.K., Dajkic, D., Kohling, H.L., von Heinegg, E.H., Fiedler, M., and Beste, C. (2017).
1043 Humans with latent toxoplasmosis display altered reward modulation of cognitive control. *Sci*
1044 *Rep* 7, 10170.
- 1045 Suzuki, Y., Wang, X., Jortner, B.S., Payne, L., Ni, Y., Michie, S.A., Xu, B., Kudo, T., and
1046 Perkins, S. (2010). Removal of *Toxoplasma gondii* cysts from the brain by perforin-mediated
1047 activity of CD8+ T cells. *Am J Pathol* 176, 1607-1613.
- 1048 Torrey, E.F., and Yolken, R.H. (2003). *Toxoplasma gondii* and schizophrenia. *Emerg Infect Dis*
1049 9, 1375-1380.
- 1050 Vyas, A. (2015). Mechanisms of Host Behavioral Change in *Toxoplasma gondii* Rodent
1051 Association. *PLoS pathogens* 11, e1004935.
- 1052 Wang, X., Zhang, C., Szabo, G., and Sun, Q.Q. (2013). Distribution of CaMKIIalpha expression
1053 in the brain in vivo, studied by CaMKIIalpha-GFP mice. *Brain research* 1518, 9-25.
- 1054 Watts, E., Zhao, Y., Dhara, A., Eller, B., Patwardhan, A., and Sinai, A.P. (2015). Novel
1055 Approaches Reveal that *Toxoplasma gondii* Bradyzoites within Tissue Cysts Are Dynamic and
1056 Replicating Entities In Vivo. *MBio* 6, e01155-01115.
- 1057 Wilking, H., Thamm, M., Stark, K., Aebischer, T., and Seeber, F. (2016). Prevalence, incidence
1058 estimations, and risk factors of *Toxoplasma gondii* infection in Germany: a representative, cross-
1059 sectional, serological study. *Sci Rep* 6, 22551.
- 1060 Wilson, E.H., and Hunter, C.A. (2004). The role of astrocytes in the immunopathogenesis of
1061 toxoplasmic encephalitis. *Int J Parasitol* 34, 543-548.
- 1062 Wyman, C.P., Gale, S.D., Hedges-Muncy, A., Erickson, L.D., Wilson, E., and Hedges, D.W.
1063 (2017). Association between *Toxoplasma gondii* seropositivity and memory function in
1064 nondemented older adults. *Neurobiology of aging* 53, 76-82.
- 1065 Xie, L., and Yang, S.H. (2015). Interaction of astrocytes and T cells in physiological and
1066 pathological conditions. *Brain research* 1623, 63-73.
- 1067 Yshii, L.M., Gebauer, C.M., Pignolet, B., Maure, E., Queriaux, C., Pierau, M., Saito, H., Suzuki,
1068 N., Brunner-Weinzierl, M., Bauer, J., and Liblau, R. (2016). CTLA4 blockade elicits
1069 paraneoplastic neurological disease in a mouse model. *Brain : a journal of neurology* 139, 2923-
1070 2934.
- 1071 Zhang, Y.H., Chen, H., Chen, Y., Wang, L., Cai, Y.H., Li, M., Wen, H.Q., Du, J., An, R., Luo,
1072 Q.L., *et al.* (2014). Activated microglia contribute to neuronal apoptosis in Toxoplasmic
1073 encephalitis. *Parasit Vectors* 7, 372.
- 1074
- 1075

Figure 1

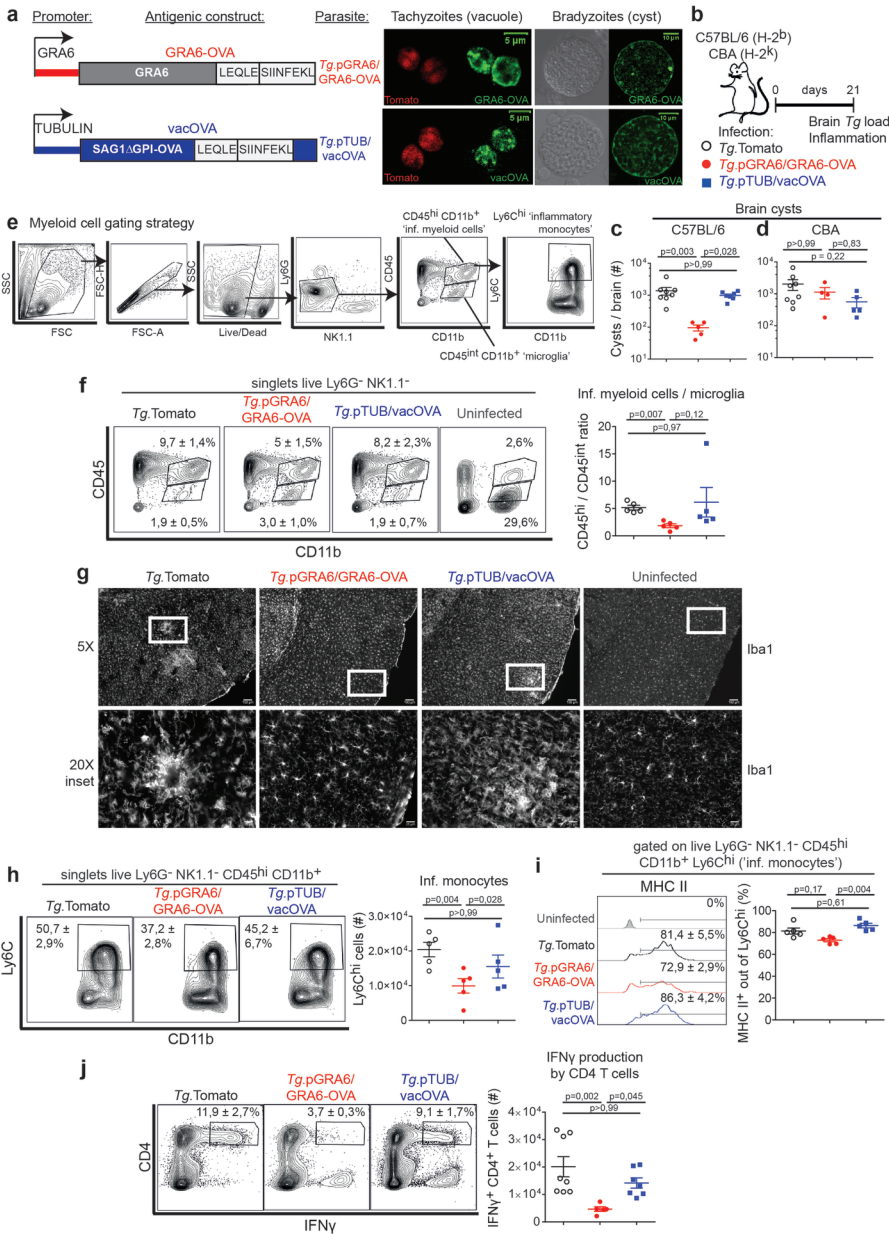


Figure 2

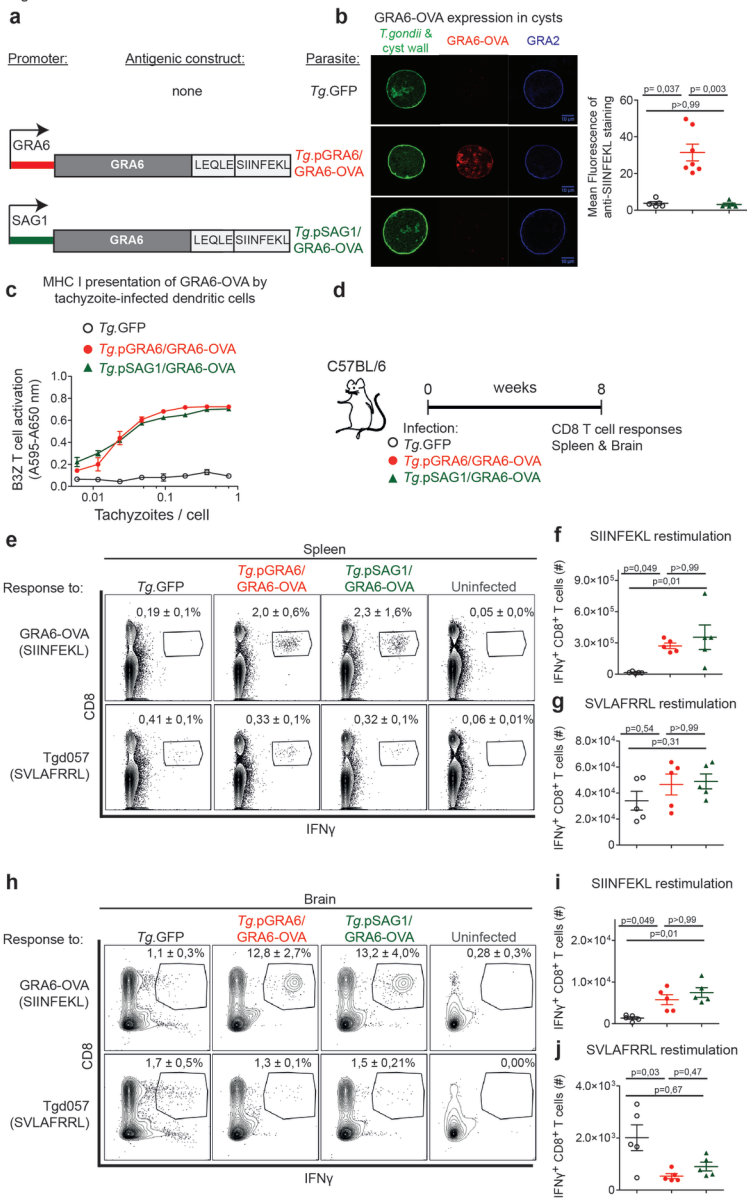


Figure 3

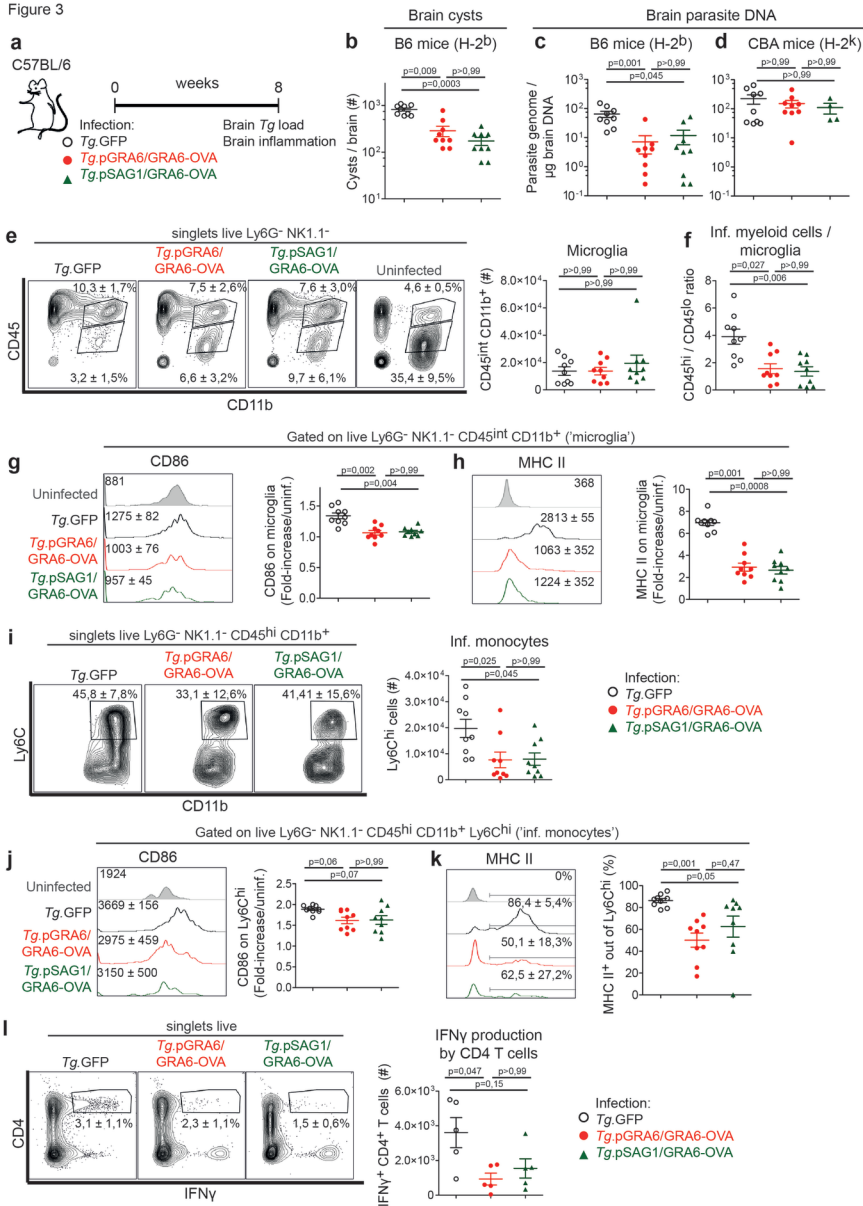


Figure 4

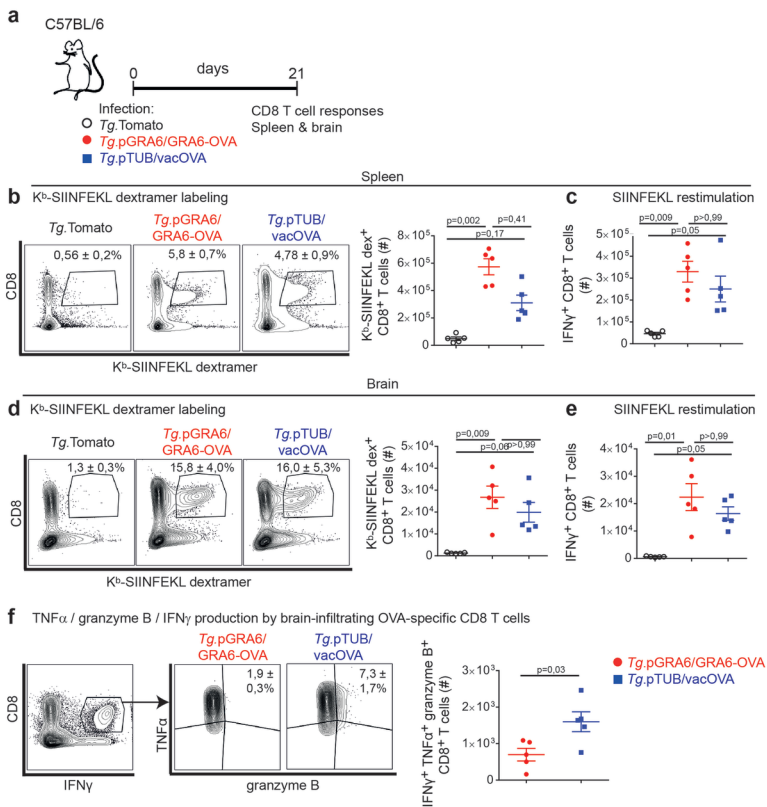


Figure 5

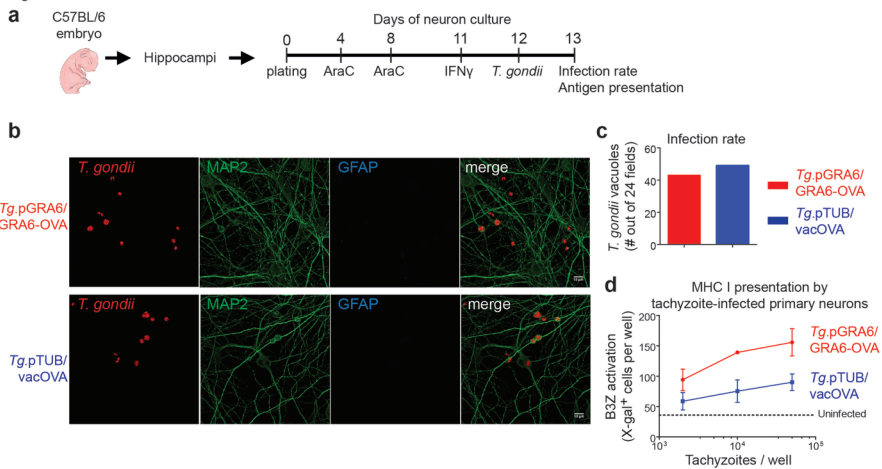
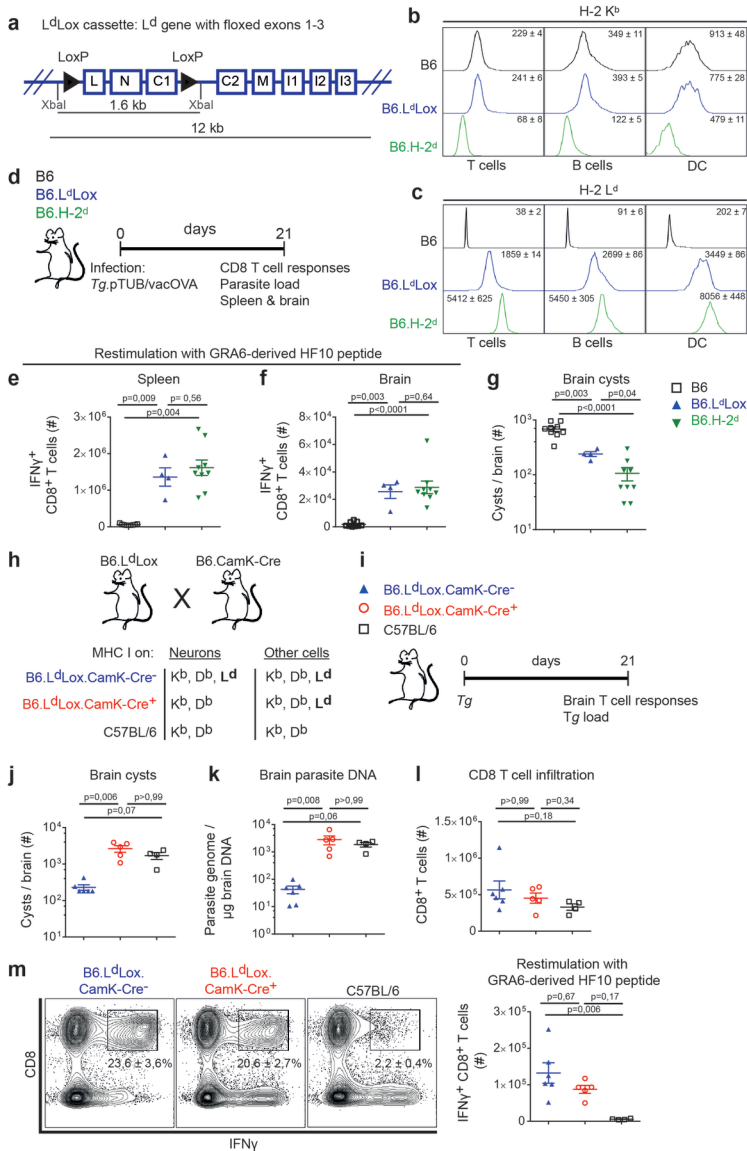


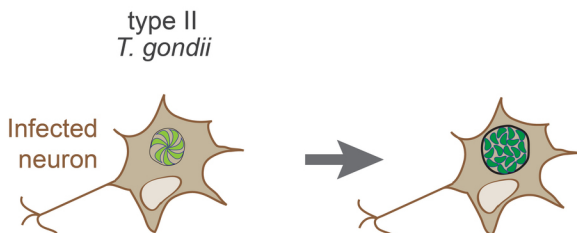
Figure 6



Early chronic (10-21 dpi)

Late chronic (> 21 dpi)

POOR
parasite
control



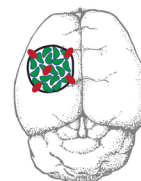
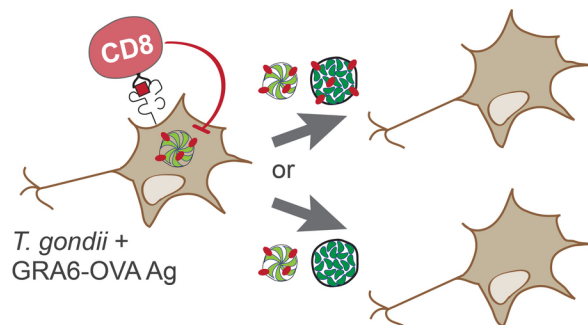
Parasite
burden in CNS



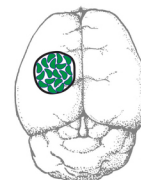
Inflammation
in CNS
(encephalitis)

+++

EFFICIENT
parasite
control

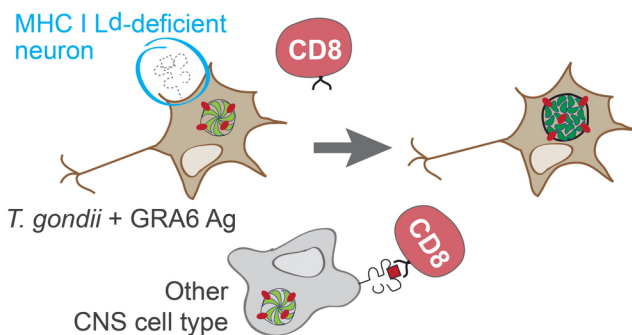


+



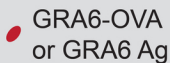
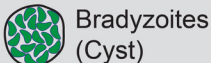
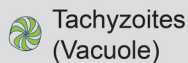
+

POOR
parasite
control



++

LEGEND



CD8

